IMPROVED MACHINING STABILITY THROUGH EDDY CURRENT DAMPING

IMPROVED MACHINING STABILITY OF THIN-WALLED ALUMINUM PARTS THROUGH EDDY CURRENT DAMPING

BY

EMMA BADOWSKI, B.Eng.

A THESIS

SUBMITTED TO THE DEPARTMENT OF MECHANICAL ENGINEERING

AND THE SCHOOL OF GRADUATE STUDIES

OF MCMASTER UNIVERSITY

IN PARTIAL FULFILMENT OF THE REQUIREMENTS

FOR THE DEGREE OF

Master of Applied Science

Master of Applied Science (2015) McMaster University

(Mechanical Engineering) Hamilton, Ontario, Canada

TITLE:	Improved Machining Stability of Thin-Walled Aluminum Parts through Eddy Current Damping
AUTHOR:	Emma Badowski B.Eng., (Mechanical Engineering) McMaster University, Hamilton, Canada
SUPERVISOR:	Dr. Stephen Veldhuis
NUMBER OF PAGES:	1, 94

Abstract

Higher efficiency can be achieved during machining of thin-walled parts while maintaining quality of surface finish by damping part vibrations, thereby increasing the maximum chatter-free depth of cut over a range of spindle speeds. Models exist both to characterize the effect of damping in machining and to quantify the result of incorporating eddy current damping on a simple vibrating cantilever beam. Impact testing was performed on undamped and magnetically damped cantilever beams to quantify the amount of damping introduced by the magnet configuration being used. Machining tests were carried out on thin-floored compliant parts with and without magnetic damping. The use of magnets during machining resulted in cutting forces reduced by a factor of 10 and surface R_a being reduced by a factor of 25.

Acknowledgements

There are many people without whom I would not have been able to complete the research contained here, and I am immensely grateful to them.

Thank you to my supervisor, Dr. Stephen Veldhuis for his guidance and support. It is because of him that I became interested in manufacturing, and his excellent supervision as an undergraduate summer researcher prompted me to pursue graduate studies.

Thank you also to Terry Wagg, Brady Semple, Joe Span, and everyone in the McMaster Manufacturing Research Institute for sharing their time and expertise. I have been privileged to work with such skilled and helpful colleagues.

I appreciate very much the love and support of my parents and all my family, who have encouraged and inspired me.

Finally, I am grateful to Matt and Holly. Their friendship and confidence in me has kept me motivated.

To my grandfather, in whose footsteps I am privileged to follow.

Contents

List of Tables

List of Figures

Abbreviations and Symbols

δ	Logarithmic Decrement
ω_n	natural frequency
θ	Tooth Angle with respect to Positive X Axis
ζ	Damping Ratio
a	Acceleration
B	Magnetic field
b	Depth of Cut
c	Damping Coefficient
d_x	Deflection in X Direction
d_y	Deflection in Y Direction
d_z	Deflection in Z Direction
F_n	Normal Cutting Force
F_t	Tangential Cutting Force

F_x	X Direction Cutting Force
F_y	Y Direction Cutting Force
F_z	Z Direction Cutting Force
h	Uncut Chip Thickness
I	Moment of Inertia
k	Stiffness
m	Mass
t	Time
v	Velocity
ECD	Eddy Current Damping
EMF	Electromotive Force
FRF	Frequency Response Function
SLD	Stability Lobe Diagram

Chapter 1

Introduction

The machining of thin-walled or thin-floored parts is common in many industries, including aerospace, automotive, and optical. Common compliant components include aerospace frames, turbine blades (figure 1.1), gear boxes (Eksioglu *et al.*, 2012), ribs, stringers, spars, bulkheads (Campa *et al.*, 2007), and other monolithic aircraft components (Tang and Liu, 2009; Song *et al.*, 2009).

Thin-walled parts can be challenging to machine as their low compliance can easily allow excessive vibration. Low forces associated with low material removal rates are often necessary to lessen vibration and ensure parts remain within the geometric tolerance and surface finish requirements. This can be a problem as it is becoming increasingly common to start with a large block of material and remove up to 95% of it to achieve a finished part with specific material properties (Campa *et al.*, 2007). This practice is desirable as it avoids non-homogeneity in the material caused by skin effects. However, for it to be viable from a productivity standpoint, it is necessary to achieve high material removal rates while avoiding chatter marks that will require additional labor to remove (Tang and Liu, 2009).

Figure 1.1: Example of thin-walled part: turbine blade

An intuitive strategy to avoid using overly low material removal rates is to increase the stiffness of the thin-walled part through fixturing strategies. While this may allow increased material removal rate, it can lead to tolerance problems. When high clamping forces are applied to a part, they induce stress and cause deformation. The part is then machined to its nominal shape and size. When the clamps are removed, the stress relaxes and the part may deform out of tolerance (De Meter *et al.*, 2001). An illustration of this process can be seen in (figure 1.2). Around 50% of part errors are caused by clamp-induced displacement (De Meter and Hockenberger, 1997). In order to avoid these problems, the 3-2-1 or the 4-2-1 fixturing principle is generally used: the workpiece is constrained by three (or four) locators in one plane to remove one translational and two rotational degrees of freedom, then by two locators in an orthogonal plane to remove another translational and rotational degree of freedom, and a final locator in a third plane removes the last degree of freedom (1.3). Finally,

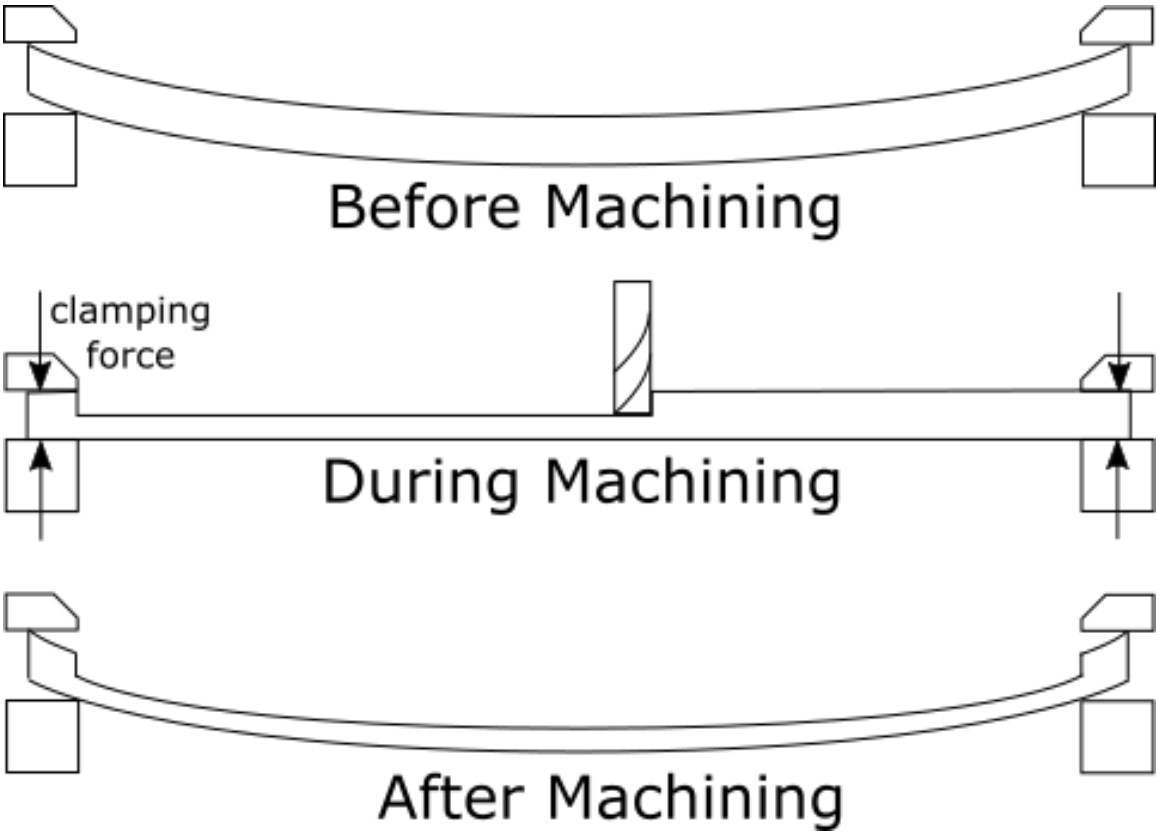

Figure 1.2: Deflection after machining of an excessively clamped part

the minimum required clamping forces to restrain the part can be calculated and applied (Li and Melkote, 2001a; Kaya, 2006; De Meter *et al.*, 2001). This method, while avoiding clamp-induced deformation problems, does not help avoid chatter in compliant parts.

A better way of avoiding chatter vibrations is to add damping. This removes vibration energy from the system leading to higher allowable depths of cut, and therefore greater material removal rate while maintaining the same surface finish and tolerances without over-constraining the part.

One way in which damping may be added to machining systems is through the application of eddy currents. Magnetic field-generating eddy currents are formed

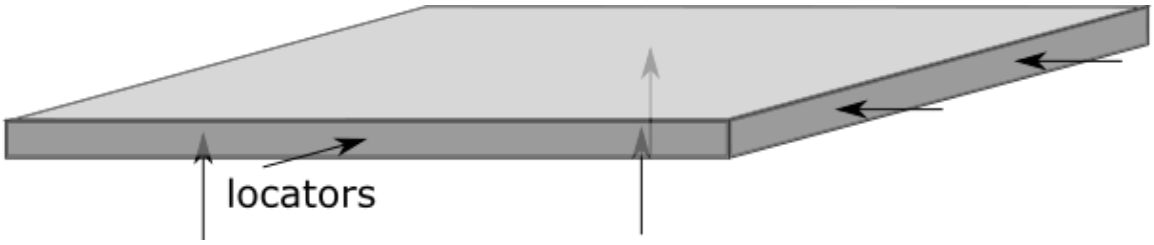

Figure 1.3: The 3-2-1 principle for workpiece location: three locators locate the part in the vertical direction, then two on the right side, then one on the front

when an area in a conductive material is subjected to a change in magnetic field. The change in field strength causes the electrons in the conductive material to move in circular eddy currents. The change in magnetic field can occur either due to motion of the conductor through a constant magnetic field, which generates what is referred to as a motional electromotive force (EMF), or due to a magnetic field of changing strength being subjected on a static conductor, which generates a transformer EMF. The circular motion of the electrons generates a magnetic field which opposes the initial magnetic field. The interaction between the two magnetic fields results in a force on the conductor, which can either attract it to or repel it from the source of the magnetic field, in the case of a transformer EMF, or slow the conductor in the case of a motional EMF.

Since the force generated by a constant magnetic field and a moving conductor will always oppose the direction of motion of the conductor, the force has the effect of damping conductor vibration. From an energy perspective, the generated eddy currents dissipate energy in the form of heat as they move through the imperfect conductor. The faster the motion of the conductor, the greater the damping effect will be. This can be beneficial in machining since this dissipated energy might otherwise cause excessive vibrations. The application of eddy current damping does not require

the workpiece to be rigidly fixed to the table in any additional locations. Since higher frequency vibrations are damped preferentially, machining-induced stress in the workpiece will still be allowed to relax naturally during machining, but problematic chatter vibrations will be damped out.

In order to predict the effects of damping on the machining process, the process must first be analyzed and understood. A great body of literature seeks to do this. Models have been created to predict cutting forces and stability behaviour accounting for factors of increasing complexity including surface roughness due to previous tooth passes, cutter and workpiece compliance, change in system dynamics as workpiece material is removed, and the effects of tool wear on cutting stability. Of particular interest to the present study is the work on systems with highly compliant workpieces, and those which examine factors affecting damping. A number of strategies are used in the literature to solve for the behaviour of the system, including analytical methods, numerical time and frequency domain simulations, and finite element methods.

Principles of part fixturing have also received considerable study. The goals of fixtures are to accurately locate the workpiece and restrain it during machining, while minimizing its deflection (Sakurai, 1992). Models have been created to aid in the selection of fixture element locations and clamping forces to achieve these goals. Numerical simulations and more novel techniques such as genetic algorithms and neural networks have been employed.

Some research also focuses on other factors affecting surface finish. The total surface profile of a part is the superposition of a number of waves of decreasing size, each caused by different factors (Benardos and Vosniakos, 2003). Approaches to predicting surface finish have focused on the use of machining theory, experimental methods,

and artificial intelligence methods such as neural networks and genetic algorithms. Factors that have been identified as having an effect on surface finish include machining parameters such as feed rate, cutting speed, and depth of cut, tool material and geometry, workpiece material and geometry, and cutting phenomena such as friction and vibration.

Considerable study of eddy currents has been conducted for general applications and in many fields outside of machining. Research on eddy current damping applications falls into three main categories: braking, rotary machinery, and dynamic systems (Sodano and Bae, 2004). The application to dynamic systems is of the greatest interest in machining. Cantilever beams represent a common configuration used to study the effects of damping. Several interesting strategies have been used to increase the damping effect of magnets, including the use of various magnet configurations to redirect the field in a beneficial way (Ebrahimi *et al.*, 2010), and the use of passive-active and active systems in addition to purely passive ones (Sodano, 2005). While most of the literature uses the optimal magnet configuration in which the motion of the conductor is perpendicular to the surface of the magnet pole, some focuses on the possibility of a less desirable but logistically necessary case in which the conductor is moving towards and away from the pole (Sodano *et al.*, 2005, 2006b).

Recently, several studies have sought to apply eddy current damping to machining through the attachment of an external damper device to the workpiece (Yang *et al.*, 2015b,a). There are several limitations associated with the work on this topic to date. The goal of the research contained herein is to further this study by examining the application of different magnet configurations to machining.

In the following chapters, the relevant literature to date on the topics of machining,

fixturing, part quality, and eddy current damping models, summarized above, will be described in greater detail. Numerical models which have been created for predicting the behaviour of an eddy current damped machining scenario will be discussed, and the simulated results will be presented. The results of cantilever beams tests for several different magnet configurations will be described. The cantilever beam test results have been used to select a magnet configuration for a machining trial, the results of which will also be presented and compared to the numerical simulation results to highlight the potential of this technology. Finally, a summary of the results and recommendations for future work will be made.

Chapter 2

Background

2.1 Modelling Machining Dynamics

2.1.1 Machining Vibration Models

Much of the work on modelling chatter in machining is based on the work of Tlusty and Ismail (1981). They described the inherent non-linearity present in machining forces which occurs when vibrations are great enough to cause the tool to jump out of the cut, reducing the force momentarily to zero. They created a numerical time-domain model to predict machining forces based on the chip thickness resulting from the current position of the tool due to vibrations, and the surface left by the vibrations during the three previous tool passes. The surface vibrations due to previous tooth passes affect the chip thickness (figure 2.1) and therefore the cutting forces. Based on the vibration non-linearity, they were able to predict with their model the maximum amplitude of vibrations that would occur based on the difference between the chip width and a limiting stable chip width. The model uses a constant process damping

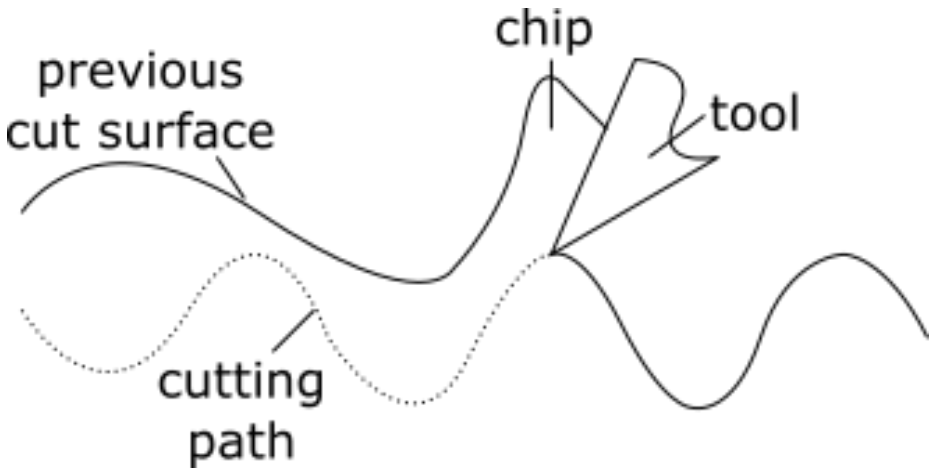

Figure 2.1: The surface left by the previous tooth pass, along with the current tool vibration, determines the uncut chip thickness (adapted from Altintas and Budak (1995))

ratio of 0.05, and accounts only for the compliance of the tool; the workpiece is assumed to be perfectly rigid.

Altintas and Budak (1995) used a Fourier series expansion of the milling force coefficients in order to predict chatter stability analytically, and achieved similar results to the numerical simulations previously explored.

Ahmadi and Ismail (2010b) constructed and experimentally validated a time domain model to predict chatter during flank milling. The model calculates instantaneous feed rate at the tool edge in order to determine the uncut chip thickness. They analytically determined the entry and exit angles based on part geometry, accounting for the 3D surface left behind by the previous tooth pass. Tool stiffness and damping in the X and Y directions were considered, and a constant damping coefficient of 0.2 was used. The tool was modelled as a lumped mass since the depth of cut was low compared to the length of the tool. The force on each tool element was determined based on the specific material removal energy and chip volume. The determination

of 3D chip geometry in this study was very detailed compared to many other works.

A review paper on the literature to date focusing on machining chatter was conducted by Quintana and Ciurana (2011). They identified three types of vibration: free, forced, and self-excited. Primary chatter was said to be caused by the cutting process, including frictional, thermo-mechanical, and mode coupling effects. Secondary chatter was said to be caused by regeneration of waviness, which is the dominant contributor to chatter vibrations. The addition of process damping results in high allowable depth of cut at low cutting speeds. The generation of a stability lobe diagram is based on the frequency response function of the system, the cutter, the workpiece material, and the radial immersion; this diagram allows spindle speed and axial depth of cut to be selected in order to generate stable cutting. The authors identified four categories of chatter avoidance strategies: selecting chatter-free cutting parameters from the stability lobe diagram using either out-of-process or in-process strategies, and changing the system behaviour in order to modify the stability lobe diagram using either active or passive strategies. Out-of-process strategies predict stable cutting conditions ahead of time, while in-process strategies sense chatter during cutting and immediately adjust the cutting parameters to eliminate it. Passive strategies involve modifying elements of the machine tool, while active strategies involve either absorbing or supplying energy from or to the system.

Quintana and Ciurana (2011) discussed a number of out-of-process chatter avoidance methods. One used delay differential equations to mathematically model chatter. A zeroth order approximation was used to approximate small cutting force variation using the zeroth order Fourier term, which allows an accurate stability lobe diagram

to be generated. The delay differential equations were converted into a series of ordinary differential equations with known solutions using semi-discretization methods. Structural dynamic tests were used to identify the transfer function. These tests were in the form of impact hammer tests using displacement, velocity, and acceleration sensors to measure the response of the system. Generation of a stability lobe diagram also requires knowledge of the cutting coefficients obtained from force measurements in the feed and normal directions during cutting. CutPro (Manufacturing Automation Laboratories Inc, 2011) can be used to calculate a stability lobe diagram from the frequency response function of the system combined with cutting test information. One difficulty that arises from impact testing is that the mass of the accelerometer used to measure the system response can significantly affect the resulting stability lobe diagram. The complexity of the model can be increased by adding elements like gyroscopic effects of the rotating spindle at high speeds, helix angle, and tool run-out. The influence of process damping is also significant, especially at low speeds. Any errors in cutting coefficients, stiffness, or damping proportionally affect the calculated limiting depth of cut. Finite element analyses can be used to predict machine tool behaviour and generate stability lobe diagrams. This can aid in the design process by ensuring prior to manufacturing that any design changes result in a part that can still be machined without chatter. Thin-walled parts present additional challenges as they result in the dynamic effects of the workpiece becoming more significant.

Quintana and Ciurana (2011) acknowledge that out-of-process strategies can be difficult to carry out in industry as they require extensive analysis prior to machining for each machine tool/cutting tool/material combination. In-process strategies eliminate this need. Parameters such as deflection of the workpiece, generated sound, and

spindle power can be measured during cutting in order to detect chatter. The spindle speed can then be adjusted to eliminate the chatter. Microphones were found to be a popular method of chatter detection in the literature, but the results can be effected by noise coming from other machines in a factory. This problem can be somewhat controlled through signal processing techniques. There are several limitations of in-process techniques. Rather than preventing chatter, they take action to stop it once it has already begun. This leaves the potential of damage to the machine, cutting tool, or workpiece before the chatter can be corrected. This technique is therefore not suitable for finishing operations. In-process techniques also require expensive equipment which cannot be shared between machines as it is used throughout the entire machining process.

Quintana and Ciurana (2011) provide limited discussion of passive chatter reduction strategies. The goal of passive strategies is to enlarge the stable zone of the stability lobe diagram by changing the system behaviour. This can be achieved by adding a damping mechanism, such as a dynamic vibration absorber or friction damper, in order to absorb energy. Alternatively, there exist special cutting tools with variable pitch or helix angle designed to increase process damping. The authors describe these as being uncommon in industry and propose lack of exposure as a reason for this.

Finally, Quintana and Ciurana (2011) discuss active strategies for chatter avoidance. These methods require that the dynamic state of the machine be monitored in order to diagnose problems and execute a solution. The vibration behaviour may be changed in various ways. For example, a delayed resonator can be used to suppress vibrations, electrostatic and piezoelectric spindle bearing supports can be used to

modify the modal properties of the machine, or active eletromagnetic dampers can be used to counteract vibrations. Some studies vary the spindle speed to disrupt regeneration effects. This works on the same principle as the use of variable helix angle or pitch tools, but is more flexible. However, spindle speed variation is more effective at low spindle speeds. In order to improve its utility, variable spindle speed can be used in combination with other methods. This is done by detecting chatter and then using information from the stability lobe diagram to decide whether to change the spindle speed to a stable value or begin continuous spindle speed variation. It can be difficult, however, to vary the spindle speed while remaining in an acceptable speed range based on the limitations of the cutting tool.

Active damping devices can also be used to inject energy into the system to compensate for vibrations. In this case, actuators controlled by computers apply given forces or displacements to counteract the vibrations. Various dampers are also described: in one study, an accelerometer is used to measure vibrations and feed information to an active mass damper. Non-linear tuned mass dampers are found to be more effective than linear tuned mass dampers for vibration suppression. Flexible plates can be machined through the use of simultaneous double-sided milling. The excessive regenerative effects caused by this method can be mitigated by running the tools at different speeds. Finally, the use of a magnetorheological fluid damper is described. In this case, the strength of the magnetic field is varied in order to actively change the stiffness.

2.1.2 Compliant Workpiece Models

A number of studies focus specifically on modelling the machining process in cases where the workpiece compliance is significant. Rivin and Kang (1989) accounted for the stiffness of both the tool and the workpiece during a turning operation. The vibration was measured using an accelerometer located at the tail stock, and the chatter frequency was determined by measuring the roundness of the machined surface. Vibration frequency was found to vary along the bar due to changes in stiffness. The system was modelled as two masses representing the cutter and the workpiece, each with stiffness and damping constants. The authors determined that there exists an optimum stiffness and tool-workpiece frequency ratio to promote stable conditions under the least amount of damping, and that the optimum values depend on the system parameters and damping ratio. Adding damping to the tool was not found to be very effective when the tool stiffness was very high. The authors claimed that higher workpiece stiffness results in better stability. While this may be true, it is not always possible to stiffen the workpiece without causing other complications. The cylindricity of the machined part was found to be improved when the stiffness of the tool was lower. The authors concluded that the best results would be achieved by reducing the tool stiffness and increasing the damping. They tested this using a tool with lower stiffness which incorporated a high damping rubber material. The maximum vibration was reduced by about half in the workpiece and tripled in the tool under these conditions, and approximately a 20% improvement in cylindricity was observed. The improvements were found to be greater at higher cutting speeds.

Liu and Cheng (2005) proposed a new way of modelling cutting forces, similar to previous work, but accounting for the dynamics of the workpiece. Their experimentally validated model showed that the surface roughness on the machined part is less than the magnitude of the tool vibrations. In other words, large vibrations of the tool do not necessarily cause poor surface finish if the cutting is chatter-free. They found surface roughness on the machined part to be more strongly influenced by cutter run-out.

Campa *et al.* (2007) looked at the machining of aerospace parts, which involve thin walls and webs in parts such as ribs, stringers, spars, and bulkheads. These parts are notable in that up to 95% of their initial weight is removed during the machining process. The high material removal rate necessary for good productivity often results in chatter which is complicated because it involves excitation of the part, not just regenerative cutting forces. Prior to this point, little work had been done on thin floor machining. The chatter problems inherent to thin floor parts are usually solved through rigid fixturing. The authors examined the machining of a pocket with a 3mm wall and a 1mm floor, as seen in figure 2.2. They used finite element analysis to calculate the modal properties of the part, and an analytical model to predict the stability of the wall and floor. They generated a 3D stability lobe diagram, which resembled a traditional stability lobe diagram extended along the tool path, and accounting for the changes in geometry as the part was machined. Cutting tests were performed based on the stability models. The authors concluded that due to the changing modal parameters throughout material removal, the spindle speed must be varied in order to maintain stable conditions.

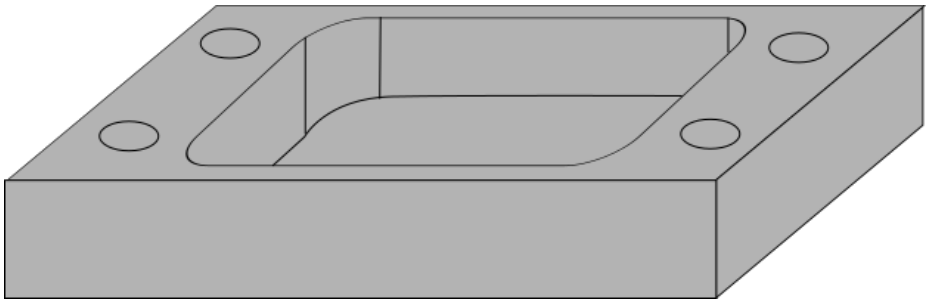

Figure 2.2: Thin-walled and thin-floored workpiece, adapted from Campa *et al.* (2007)

Song *et al.* (2009) modelled high-speed machining of a thin-walled workpiece with a tool assumed to be rigid. An analytical analysis was performed on a prismatic aluminum workpiece to generate a model. The differential delay equation approach was used to model the machining process, accounting for the time delay and variable parameters due to material removal. Eddy current displacement sensors were used to measure one-dimensional displacement during the cutting tests. The modal parameters were measured using impact hammer testing prior to the cutting tests. The semi-discretization method was used to find a 3D stability lobe diagram describing the change in stability conditions as the tool moved along the cutting path and material was removed. The tests were performed without coolant, and the motivation for this decision during cutting of aluminum was not discussed. The agreement of the experimental results and the model predictions was not clearly described.

Tang and Liu (2009) analytically generated a 3D stability lobe diagram for up milling of a thin cantilever beam with a rigid tool. The variation in modal parameters as material was removed was neglected, and the third axis of the stability lobe diagram instead showed variation in radial depth of cut. The workpiece was assumed to deflect uniformly, neglecting the possibility of greater deflection at the tool location. The stability lobes were found to start high at very low radial immersion, then decrease

rapidly as the radial immersion was increased, and finally increase to full immersion. The maximum stable material removal rate occurred during full radial immersion. This may be because during full immersion, some of the cutting forces cancel out and do not contribute to unstable vibration. Additionally, the greater contact area during full immersion likely leads to higher process damping.

Eksioglu *et al.* (2012) created a milling model which accounted for the flexibility of both the tool and the workpiece. Stability was assessed by checking whether vibration was growing exponentially. Their milling simulation allowed for the use of various tool and workpiece geometries, including accounting for run-out in the tool, helical, ball nose, and bull nose tools, tools with serrated edges, variable tooth pitch and helix angles, and indexed cutters. The model also accounted for vibration in all three directions. Process damping was calculated using the volume of elastically deformed material at the flank face of the tool. The model distributed forces to nodes placed along the tool and workpiece in order to account for their compliance. The simulation employed delay differential equations solved using the semi-discretization method. The model was experimentally validated using a high axial and small radial depth of cut.

2.1.3 Modeling Process Damping

A number of studies focus on modelling the amount of inherent process damping which will occur during a machining operation based on the system parameters and tool geometry. Lee *et al.* (1995) focused on process damping which occurs at the interface between the flank face of the tool and the machined surface of the workpiece. They postulated that damping was caused by ploughing of the workpiece material

as the tool moves through the waves left on the machined surface by previous tool vibration. The resistance force from ploughing was said to be proportional to the volume of material displaced, allowing the damping force to be predicted through numerical simulation. Their model uses a neural network to model cutting forces, with inputs of uncut chip thickness, chip width, cutting speed, and rake angle, and outputs of cutting and tangential forces. They noted that a steeper slope on the wavy cut surface occurs under lower cutting speed, which results in more interference between the tool and the workpiece and therefore a higher damping force (figure 2.3). They account for the surface left only by one previous tooth. They claim that stability in cutting is primarily caused by the non-linear damping force, rather than by the tool jumping out of the cut. They found low cutting speed to result in greater stability due to increased damping.

Altintas *et al.* (2008) investigated the influence of the interaction between the cutting edge and flank face contact with the wavy machined workpiece surface on cutting forces and stability in turning. They were particularly interested in low speeds, where stability lobe models tend to agree poorly with cutting test results. As tool wear affects process damping, they measured cutting coefficients using both new and worn tools. Their model accounts for tool wear by using different cutting force coefficients when simulating tools at different stages of wear. The model was found to more accurately predict stability of tools under different wear conditions, particularly at low speeds.

Rahnama *et al.* (2009) examined the effects of process damping on chatter suppression in micro end milling. Process damping is an especially important consideration in micro machining since size effects influence the results. Generally more ploughing

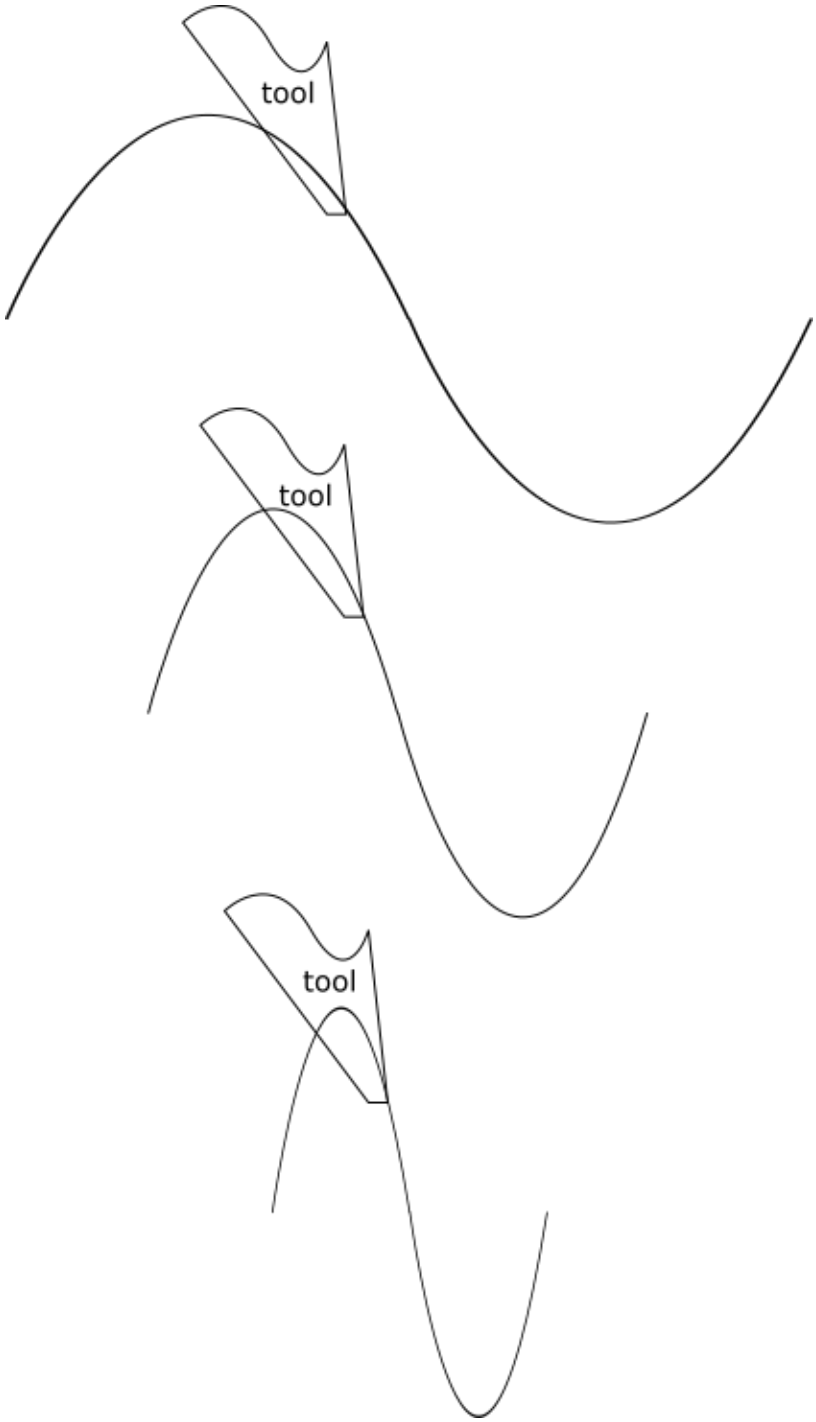

Figure 2.3: Lower cutting speed (bottom) results in steeper slope on surface waves and more tool-workpiece interference, adapted from Lee *et al.* (1995)

occurs due to the relatively larger cutting edge radius compared to the chip thickness. The authors projected the X and Y directions onto one plane to create a pseudo one degree of freedom system in order to facilitate an analytical model. As is common in the literature, they assumed the process damping was proportional to the volume of ploughed material. They calculated a ploughing coefficient based on the experimentally measured cutting forces. Scanning electron microscope images were used to measure the tool edge radius in order to account for it in the ploughed material volume calculations. Modal properties of the tool were determined using finite element methods. A stability lobe diagram was generated for the process and it was found to be in good agreement with experimental results, showing a significant improvement over previous models, especially in the low spindle speed region.

Ahmadi and Ismail (2010a) focused on the nonlinearity of process damping. They postulated that the reason for poor stability prediction at low speeds in many stability lobe diagrams is due to the failure to account for damping generated by cutter-workpiece interaction, and particularly the ploughing force. They determined that process damping depends on the workpiece material, the tool clearance angle, tool wear, cutting speed, and feed rate. They accounted for process damping in their machining model using a complex cutting coefficient where the imaginary part represented the damping. The workpiece was assumed to be totally rigid and the tool was assumed to be rigid in all but the normal direction. They modelled an uninterrupted cutting process, as in turning. As is common, they calculated the ploughing force based in the volume of displaced material. They found that when process damping was accounted for, the transition from stable to unstable cutting as depth of cut was increased happened very gradually.

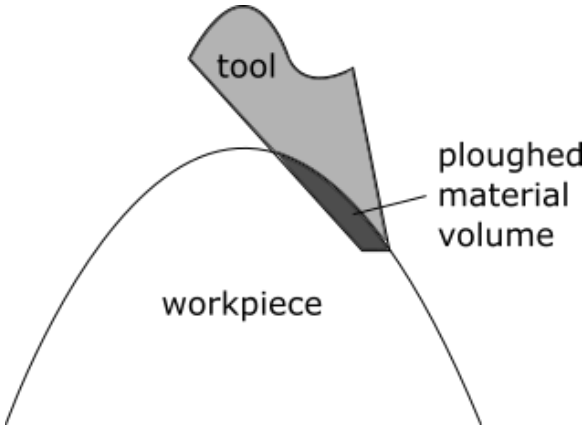

Figure 2.4: Displaced material during ploughing, adapted from Ahmadi and Ismail (2010a)

Budak and Tunc (2010) examined a different approach for modelling process damping in both turning and milling. They used an average coefficient for damping in the equation of motion for their model, which was then solved using an analytical approach. The damping coefficients were identified from both orthogonal cutting and milling tests at a variety of cutting speeds. They then validated their model using both numerical simulations and experimental testing. Because process damping depends on a number of parameters including workpiece material and tool geometry, this approach seems limited in that it relies on initial testing to determine the damping coefficient. This testing would need to be repeated for each tool-workpiece combination in order to accurately predict stability.

Yusoff *et al.* (2010) examined the role of tool geometry on process damping, particularly in difficult-to-machine materials. They used a four flute tool with a rigid workpiece, and a three flute tool with a workpiece mounted on a flexible fixture to allow for acceleration data to be collected. The acceleration of the workpiece was measured due to the difficulty of attaching an accelerometer to a spinning tool. The

tool edge radius was measured using a perthometer with a stylus tip. The frequency response function for the tool was generated through impact testing. Chatter onset was measured by conducting cutting tests at constantly increasing spindle speed. The authors found that higher process damping wavelengths resulted from tools with a larger edge radius, while the effect of rake angle on process damping wavelength was inconsistent.

Ahmadi and Ismail (2011) used an analytical single degree of freedom model to examine the effects of process damping on stability in machining. Their model assumed the forces present during machining to be composed of shear and ploughing components. As usual, the ploughing forces were assumed to be proportional to the volume of material deformed. A non-linearity was present due to the fact that ploughing only occurs during the portion of the vibration when the tool is moving towards the workpiece, and because the ploughing force depends on the amplitude of the vibration. Because accounting for non-linearity is computationally expensive in a numerical model, the authors used an analytical representation of damping based on the tool geometry and the previous surface shape. The process damping was then replaced with equivalent viscous damping in order to analytically generate stability lobes. Rather than the usual method of generating a single stability lobe, they determine upper and lower stability bounds to represent the transition from stable to marginally stable, and finally to unstable cutting. Their model agreed well with time domain simulations and experimental plunge turning results.

Huang and Wang (2011) developed an analytical model in which they divided the process damping into four separate forces: direction-shearing, direction-ploughing, magnitude-shearing, and magnitude-ploughing. They modelled the workpiece as a

two degree of freedom mass-spring-damper system with a rigid tool, as seen in figure 2.5. Process damping was found to have a greater effect in down milling compared to up milling. It was also found to be more effective when the cutting speed was tuned to bring the harmonic milling forces close to the resonant frequency. The predicted results were validated experimentally with good agreement. The dynamic cutting factor was found te be related to cutting speed but not feed per tooth or radial depth of cut. The authors found the process damping to increase with decreasing wavelength below a critical value, but remain relatively constant for wavelengths above this critical value.

Sellmeier and Denkena (2012) used a tool with a chamfered edge in their process damping analysis. They found this edge preparation extended the benefit of process damping at higher cutting speeds. They considered the volume of material indented by the cutting edge to create an opposing force which generates a damping effect. They used delay differential equations for initial modelling, and numerical methods for the stability analysis. The frequency response function of the system was measured through impact hammer testing. Stability was judged after machining through a visible inspection of the cut surface for chatter marks. The use of a chamfered tool was found to heat the workpiece noticeably. Experimental results can be seen to correlate poorly with predicted results for larger chamfers, but better agreement can be observed for small chamfers. Interestingly, rather than simple stability lobes, the authors found that process damping caused unstable islands to arise, which they postulated was due to regenerative effects. The general trend observed for chamfer geometry was that the process damping coefficient was found to decrease with increasing chamfer width.

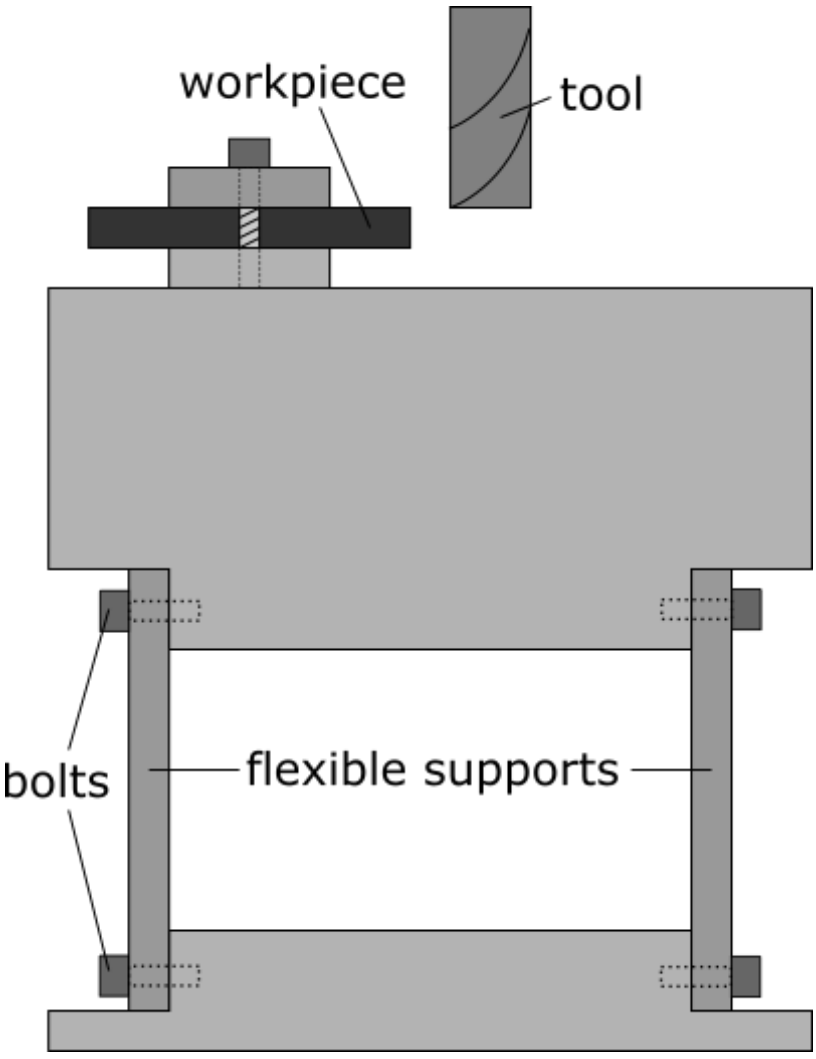

Figure 2.5: Workpiece mounted on compliant supports used in process damping machining trial, adapted from Huang and Wang (2011)

Tunç and Budak (2012) examined process damping under a variety of cutting conditions and tool geometries. They determined that the process damping coefficient can be written in terms of the actual stability limit of the system determined through empirical data, and the theoretical stability limit not accounting for process damping. This is more difficult in milling since the system has two orthogonal degrees of freedom, but it can still be accomplished using an iterative process. They postulated that the cutting face indents into the workpiece when the surfaces slope on the workpiece is greater than the clearance angle of the tool. A lower clearance angle was therefore found to produce higher process damping. Higher hone radius also produced more process damping, since higher hone radius causes more material to be extruded against the cutting tool. Increasing the flank length of the tool increased the process damping to a point, but after a critical flank length, the process damping leveled off. The authors postulated that this has to do with the length of undulations on the workpiece surface. A cylindrical flank face was found to produce more process damping than a planar one. These process damping results were used to predict limiting depths of cut, which were then validated experimentally. Higher contact length between the tool and the workpiece was generally found to increase process damping and therefore stability. The effect of this increase contact length on the quality of the machined surface was not investigated. It seems plausible that this may result in high heat in the workpiece, leading to the potential for microstructure damage on the machined surface.

2.1.4 Adding Damping

Rather than just measuring inherent process damping, many researchers have sought to add external sources of damping in order to improve the stability of cutting processes. Weck *et al.* (1999) developed a damping system to be applied to a tool holder in order to reduce chatter vibrations in the tool. Its application is most beneficial to boring processes where the length to diameter ratio must be high. They used finite element analysis to model the tool geometry using beam elements with uniform elasticity and mass, and a lumped mass at the end. Their work primarily focused on optimizing the geometry of the inner hollow in the boring bar to maximize stiffness while minimizing mass. Both steel and carbon fiber laminate boring bars were investigated. They also proposed a tool holder which used squeeze film fluid to add damping. The damped tool holder achieved a depth of cut three times higher than an undamped one while experiencing the same magnitude of vibration. The process stability was also found to be influenced by the machine tool itself, and the authors proposed a hydrostatic bearing in the spindle to increase its damping.

Suh *et al.* (2001) examined the use of spindle covers to damp machine vibrations. They used carbon fiber reinforced epoxy bonded to the thin steel plate spindle covers to absorb energy. Finite element analysis was used to find modal information about the spindle cover, and impact testing was conducted on the cover suspended by a string to determine the frequency response function. Under these testing conditions, the amplitude of vibrations was found to be decreased to about a tenth compared to the traditional spindle cover. However, the significance of this reduction during a real machining process was not examined. While significant vibration of a spindle cover, if it occurs during machining, has the potential to cause undesirable noise in

the shop, the impact of such vibration on the cutting process itself is not clear.

Duncan *et al.* (2005) sought to use the cutting parameters to induce a dynamic vibration absorber effect. They noted that the limiting depth of cut of a machining process depends on the negative real part of the tool point frequency response function. By increasing this value, the stability lobes can be shifted up. They accomplished this by tuning the frequencies of the tool and spindle holder. This theory was tested using a stacked flexure assembly, then extended to real spindle-holder-tool assemblies and validated experimentally with good results.

Ganguli *et al.* (2005) used a machining simulator to study the use of active damping to suppress chatter. They used an aluminum cantilever beam to represent a turning process, and an interferometer to measure displacement. Damping was added through an electromagnetic active mass damper to apply force to the beam. The addition of damping was shown to successfully shift the simulated stability lobes up to a higher limiting depth of cut. These results, however, were compared only to a numerical analysis, and real cutting tests were not performed.

Zhang and Sims (2005) studied the use of piezoelectric active damping to improve stability in milling. They used a cantilever beam workpiece and conducted impact testing to determine the frequency response function of the system. A piezoelectric actuator and sensor sensed vibration and actively added damping to compensate. This method was able to achieve a limiting depth of cut about four times higher than the undamped system.

Ganguli *et al.* (2007) examined the application of active damping in single degree of freedom turning. An analytical analysis of the turning process was conducted to determine stability lobes and chatter frequencies. Stability was assessed using the

root locus method. A velocity feedback loop was used to suppress vibration. While considerable discussion of the improved stability using damping was presented, no experimental results were discussed.

Wang (2011) implemented a tuned mass damper, which was tuned to minimize the real part of the system's frequency response function in order to improve stability. A tuned mass damper can dissipate energy either through internal friction of the spring material, or through friction at the interface between the damper and the structure to which it is attached. The authors used a new tuned mass damper design which involved a second spring-friction element in series in order to increase the total friction damping. The damper absorbs energy both through sliding friction and viscous damping. A numerical optimization method was used to choose the tuned mass damper parameters. Based on simulations, which assumed a compliant workpiece and a rigid tool, they calculated a 30% improvement in the critical limiting depth of cut over traditional tuned mass dampers.

2.2 Fixturing

Another topic of research in the area of machining relates to fixturing practices. The ultimate goal of fixturing is to ensure the greatest possible dimensional accuracy by choosing the number and location of fixture elements and the clamping force to prevent dislocation and deformation, both from the clamping and the machining forces.

2.2.1 Fixturing Models

Sakurai (1992) listed a number of requirements for fixturing systems. They said fixtures should locate the workpiece accurately, restrain the workpiece during machining, minimize deflection of the workpiece, avoid interfering with the machining process, and also possess a quality called "goodness", which accounts for the desire for ease of use and minimal non-machining time. Employing the 3-2-1 fixturing principle, a computer followed a series of rules based on the datum features identified in a CAD model of the part in order to choose the location of the fixture elements. The algorithm attempted to choose fixture locations to allow as much of the workpiece to be machined as possible. The workpiece was assumed to be rigid, and the dynamic behaviour of the system was not taken into account.

Li and Melkote (1999) created a method for optimizing the fixture elements accounting for the effect of clamping forces on the locational accuracy of the workpiece. They noted that their method is computationally less expensive than finite element analysis, which is often used for fixture layout optimization. The workpiece was modelled as elastic near the contact points and rigid elsewhere. The deformation from contact forces and friction at contact points was modelled, and a static equilibrium constraint was applied. The authors used a selected clamping force for the model rather than optimizing the clamping force. The positions of the fixture elements were constrained to bounded regions, and the 4-1-2 principle was applied. The system of equations was solved in MATLAB using a nonlinear programming method to optimize for minimal displacement.

Li *et al.* (2000) studied the effects of using fixtures like vises, which transmit torsional loads in addition to normal and tangential loads, instead of the more frequently

modelled spherical and cylindrical contacts. They modelled the contact region between the vise and the workpiece as four square regions, each containing a uniform pressure distribution. They solved for the applied clamping load using the minimum energy principle, then analyzed whether this was sufficient to restrain the workpiece under the forces from a given cutting scenario. They noted that this method does not necessarily result in the minimum required clamping force, but described how this figure could be determined.

Li and Melkote (2001a) focused on optimizing clamping forces, which must be high enough to restrain the workpiece, but no higher to avoid excessive deformation leading to location inaccuracy. They solved the otherwise statically indeterminate rigid body model by accounting for localized elastic deformation in the contact regions between the fixture elements and the workpiece. The system was modelled as a multi-objective constrained optimization problem, where the minimum energy principle was used as the primary objective and the minimization of clamping forces was treated as a constraint. Coulomb friction was modelled at the contact points, and the system was considered to be in quasi-static equilibrium. The forces in the clamps were constrained to be compressive, and to generate stress not exceeding the yield stress of the workpiece material. This optimization method is valid for a single applied load, so the model was extended to a machining case by dividing the tool path into a finite number of points and calculating the clamping forces based on the worst case machining forces in each orthogonal direction at each point. The final optimum clamping forces were selected by taking the maximum clamping forces found from the solutions at all the tool locations and checking them for their ability to maintain static equilibrium. This method does not account for the elevated machining forces that

could result if unstable cutting occurs. The workpiece deformation upon application of clamping forces were calculated and used to generate a transformation matrix, which could be applied to the tool path to account for displacement.

Li and Melkote (2001b) developed a method of optimizing both fixture locations and clamping forces accounting for the effects of the dynamics of the workpiece. This was accomplished by modelling the fixture contact points on the workpiece using contact elasticity. The displacement of the workpiece was assumed to be small enough not to affect the machining forces. The locators and clamps were constrained to be in contact with the workpiece and not to slip. The positions of the fixture elements were constrained to be within fixed regions. An iterative method was used to solve for the final positions and clamping forces. The positions found by the algorithm were found to be consistent with rule of thumb practices despite intentionally poor starting positions.

Kaya (2006) employed a genetic algorithm to solve for the optimal fixture element locations and forces. Their goal was to minimize the elastic deformation of the workpiece. One limitation of traditional location optimization algorithms is that they rely heavily on the initial selected layout. Genetic algorithms avoid this limitation by using random search techniques that mimic evolution. They select a population of solutions, called chromosomes and determine the fitness of each of the chromosomes. In this case, fitness was based on minimizing displacement and deformation. A new population is then created by adding mutations and crossovers to the current population based on their fitness. In this study, a library of finesses was maintained to reduce computation time in the case that the fitness of a chromosome had been calculated in a previous population. The algorithm used the 3-2-1 fixturing principle and required

the forces in all locators to be positive in order to prevent loss of contact. Friction was not considered. Finite element analysis was used to determine the deformation and displacement of a given solution, accounting for changes in geometry as material was removed during the cutting process. A benefit of the genetic algorithm method is that it provides all optimal solutions in cases like fixture locations, where there may be several. Then, the best solution can be selected from these based on previously omitted criteria such as ease of fixturing or tool path programming.

2.2.2 Compliant Workpieces

A number of studies account for the compliance of the workpiece when optimizing fixture design. Daimon *et al.* (1985) focused on fixturing thin-walled plate and box workpieces to allow them to be machined under chatter-free conditions at a target feed rate. Their definition of a "thin" workpiece is one in which the thickness is 1/100-1/200 of the maximum dimension. They sought to ensure that the compliance of the workpiece was maintained below a target allowable limit, based on numerous machining tests, at any point during machining. Their algorithm assumed the workpiece was clamped at three datums, and then searched for the minimum number of supports required to meet the stiffness criterion. Impact testing and finite element methods were then used to find the optimal support locations.

De Meter *et al.* (2001) developed a model for determining the clamping pre-loads while accounting for the compliance of the system. They first determined the compliance of the system, accounting for the workpiece, the load bearing fixture elements, and the attachment of the fixture elements to the table. Response points with three

degrees of freedom were identified at all points of load transmission between the fixture elements and the workpiece. Compliance matrices were then determined through finite element analysis to describe the relationship between the load at a point, and the translation of the point in all degrees of freedom. Next, the contact forces were modelled. Contact forces due to gravity, clamp loads, and machining forces were considered, as were the displacements of the workpiece and clamps due to gravity, clamp forces, and machining forces. The model assumed no sliding or lift-off occurred at the workpiece-fixture interfaces. A linearized model for friction was used based on the no-slip assumption and the previously calculated forces. Optimization for a single external load was carried out using commercial software. This was done for each external load case separately, and the highest resulting preloads were selected. The determined preloads were validated experimentally using a simulated machining load and test samples made of materials and with various surface finishes. The calculated optimal preloads were found to be sensitive to the compliance of the fixture elements, and the coefficients of friction between the fixture elements and workpieces with various surface finishes.

Chen *et al.* (2008) used a genetic algorithm to optimize fixture element positions and clamping forces accounting for friction and changes in geometry due to chip removal. They used a workpiece with low rigidity, unlike many previous studies. The maximal cutting force generated by a cutting model was used as an input to a finite element model. The finite element model determined the deformation of the workpiece based on this cutting force as well as clamping forces. The deformation was sent to the genetic optimization algorithm to search for the optimal clamping force. The entire tool path was simulated by applying the maximum cutting forces

in three orthogonal directions to each point along the tool path in the finite element model. The compliance of the workpiece was modified to account for the removal of material during cutting. The maximum displacement caused by the cutting force was used as the fitness value for the genetic algorithm. This neglects to account for the deformation caused by the clamping forces. The same mesh was used in the finite element model for each chromosome in the genetic algorithm, but different boundary conditions were applied to account for the fixture element positions. A multi-objective approach was input to the genetic algorithm, optimizing for minimum deformation and maximum uniformity of deformation. The algorithm presented in this study excelled compared to a single-objective method with both of these objectives.

2.3 Part Quality

2.3.1 Error Compensation

Several studies have focused on compensating for factors which result in errors in the final part rather than preventing them. De Meter and Hockenberger (1997) used a tool path compensation method to account for displacement of the workpiece during machining due to contact region deformation, slip, and lift-off. They noted that the workpiece displacement can either be predicted analytically or detected using eddy current displacement sensors, and is affected by geometry, placement, actuation intensity, and actuation sequence of the clamps and locators. The process parameters and tool path can also have an effect on errors. Workpiece displacement has been found to contribute around 80% of the total geometrical errors, with around 50% being from clamp-induced displacement. The study used spherical-tipped locators

and hydraulic clamps, and assumed the fixture and workpiece to be rigid everywhere except near the contact interfaces. Six eddy current displacement sensors were used to measure displacement of the datums in the six degree of freedom system. The sensors were placed adjacent to the locators. The displacement after application of the clamping force was measured and used to create a 6x6 matrix. This matrix was then applied to all tool paths. While this method was found to be effective in compensating for the error due to clamping force, it doesn't account for machining forces, which can cause considerable deformation in a compliant workpiece.

Ratchev *et al.* (2004) focused on compensating for errors caused by machining forces in thin-walled parts. They predicted and compensated for the deflection in an iterative process, where the cutting forces were calculated and input to a finite element model to determine the deflection of the part, which then led to changes in the cutting force calculation. The cutting tool was initially assumed to be rigid, then its deflection was incorporated later in the model. This method neglects any interaction between the dynamic properties of the cutter and workpiece which could potentially lead to unstable vibrations and increased cutting forces and deflections. Experimental validation found an 8% difference between the predicted and measured resultant forces. The resulting improvement in the accuracy of the final part geometry was unclear.

2.3.2 Surface Roughness

Other studies focus on predicting surface roughness in machining. Benardos and Vosniakos (2003) reviewed the literature to date on the subject. They described a number of types of surface topography in descending order of size, as well as their

causes. First and second order deviations, called form and waviness occur due to machine tool errors, workpiece deformation, clamping, vibration, and defects in the workpiece material. Third and fourth order deviations occur in the form of grooves, cracks, and dilapidations and occur due to the condition of the cutting edge, the chip formation process, and the kinematics of the cutting process. Fifth and sixth order deviations are related to the workpiece material structure and occur due to physical and chemical processes on a grain scale. The total surface roughness profile is a combination of all of the aforementioned types of deviation. The authors noted that relating surface roughness directly to feed rate is generally not very accurate without accounting for additional factors. Many theoretical machining models examine the effects on surface roughness of a number of factors including run-out in the tool, vibration, and tool geometry. Some researchers use various methods to predict surface finish, while others focus on using experimental methods to measure the effects of varying parameters. Tool wear, along with feed rate frequency and spindle and workpiece natural frequencies have been found to effect surface roughness. Displacement sensors, acoustic emission techniques, and ultrasound scans can be used to detect roughness during machining. Techniques such as cryogenic cooling, edge hone radius control, and various tool geometries including ball nose end mills and inclined end mills have been used to try to improve surface roughness. The relative influence of cutting velocity, feed rate, and depth of cut on surface finish has been studied by numerous researchers, with some finding velocity and others feed rate to have the greatest effect.

Lu (2008) used a neural network to predict surface finish in machining. They used cutting speed, depth of cut, and feed rate as parameters. Cutting tests on lathes

using varying parameters were conducted in order to train the neural network. The cutting tool was replaced regularly to prevent the impact of tool wear. The predicted and measured profiles were found to agree reasonably well in phase, although small variations in the magnitude and shape of the profiles suggested that there is a limit to the accuracy that can be obtained when accounting for the effects of only three possible variables.

2.4 Eddy Current Damping

Eddy current damping is a well-known phenomenon which has been studied and modelled in many contexts outside of machining. The literature describes two types of force which can be generated: motional EMF, which occurs when a conductor moves in a magnetic field, and transformer EMF, which is experienced by a stationary conductor subjected to a magnetic field with changing strength.

2.4.1 Models

A number of analysis methods have been used to predict the effects of various configurations of eddy current damping. Davis and Reitz (1971) described a drag force experienced by a magnet moving over a conducting plate, which occurs due to the fact that the magnet makes up for Joule losses in the conductor. They identified a "lift force" caused by eddy currents in a semi-infinite conducting sheet from a disk magnet. They solved for the behaviour of the system by theoretically moving the source of the magnetic field in a series of jumps and calculating the resulting eddy

currents. The jumps were then made smaller and smaller until they represented continuous motion. Because eddy currents decay over time, the speed of motion of the magnet effects the strength of the generated field. In the case of high speed movement, this decay can be neglected as the magnet has moved away before the decay becomes significant. This allows the conductor to be treated as perfect. The authors solved the system analytically using a common technique called the image method. The image method accounts for the boundary conditions of the system by creating a hypothetical opposite charge reflected across the boundary plane.

Nagaya *et al.* (1984) studied eddy current damping forces in arbitrarily shaped plate conductors. They found an analytical solution using the Fourier expansion collocation method to account for the irregular conductor shapes, and validated their solution experimentally.

Zuo (2005) examined the impact of altering the direction of a magnetic field inside a conductor. The damping coefficient for an eddy current damper is known to be $C = C_0 B^2 t A \sigma$, where B is the magnetic flux density in Tesla, t is the thickness of conductor plate in m, A is the area of the conductor in the magnetic field in m^2, σ is the electrical conductivity of the conductor in $(\Omega m)^{-1}$, and C_0 is a dimensionless coefficient related to shape and size. If the magnetic field is uniform and the conducting plate is infinite, C_0 is 1; typically it is between 0.25 and 0.4. The author used magnets with alternating field directions, and found the damping force to increase by 2.5 times compared to the same magnets all oriented in the same direction.

Das *et al.* (2008) used MATLAB to conduct a finite element analysis to determine the damping coefficient of an eddy current damper. They used a copper plate and an annular magnetic field, with motion occurring perpendicular to the magnetic field

lines. They compared the results to an externally-derived equation with good results. Experiments to validate their model were conducted, although the results were not presented.

Ebrahimi *et al.* (2010) examined the effects of various configurations of permanent magnets on eddy current damping. The magnets were mounted on springs on a track which allowed them to move through an aluminum tube. The orientations of the magnets are shown in figure 2.6. Finite element analysis was used to predict the field patterns generated by the various magnet configurations. Based on this, it was determined that the (b) configuration would cause the highest damping force of the configurations under consideration, however the (a) configuration was used in tests due to the difficulty of obtaining the necessary magnets for the (b) configuration. The motion of the magnets was measured using accelerometers, and the damping ratio was found to increase from 0.035 with no eddy current damping to 0.28 with the (a) configuration of magnets.

Niho and Horie (2010) used eddy currents to induce rather than to damp vibrations. By changing the field strength of an electromagnet in a controlled fashion, they were able to generate a force on a conductor and induce vibration. They accounted for the effects of eddy current damping slowing the induced vibration in the system. They used a one degree of freedom system to validate this theory.

2.4.2 Cantilever Beam

Cantilever beams are a common geometry to which eddy current damping is applied. Their study is of particular interest as it can easily be extended to machining workpieces. Kanamori and Ishihara (1989) conducted a finite element analysis of an

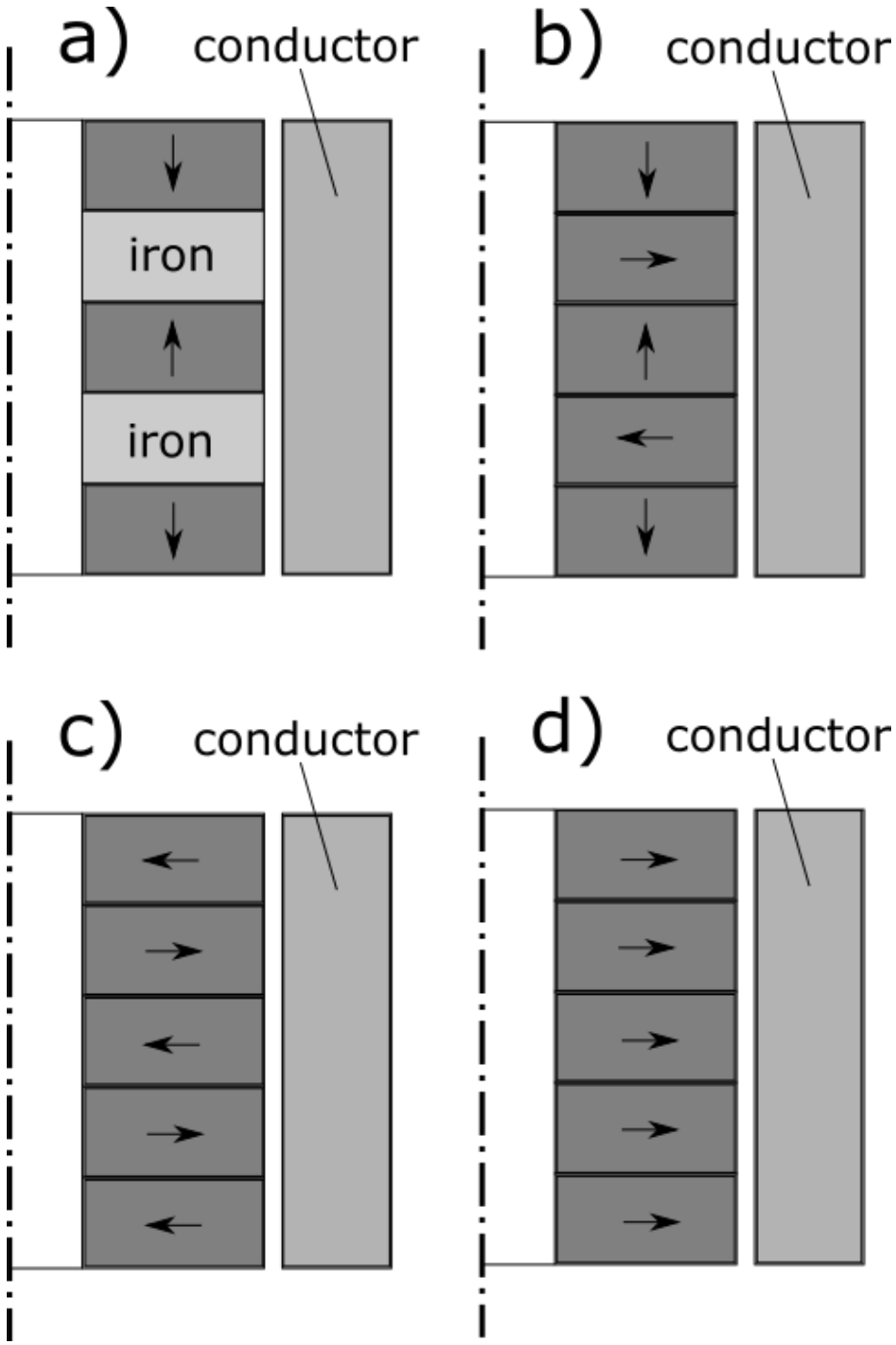

Figure 2.6: Test orientations of magnets moving through aluminum tube, adapted from Ebrahimi *et al.* (2010)

electromagnetic eddy current damper. The model was validated experimentally using a cantilever beam with a conductor slab on the end. The 5mm thick conductor moved through a 9mm gap between two electromagnet coils, with the motion perpendicular to the field lines.

Tanaka and Horie (2002) examined the effect of eddy current damping on a cantilevered copper plate in a magnetic field subjected to a harmonic force at the free end. They created a one degree of freedom model and performed finite element analysis to predict the behaviour of the system.

Bae *et al.* (2005) created a theoretical model for eddy current damping in a cantilever beam using the image method to account for the end effects. The authors used a linearly varying velocity in the x-direction in their model to simulate the pendulum-like motion of a cantilever beam. The vibration was, as in most of the previous works, perpendicular to the magnetic field lines. The results from the model were compared to experimental data from a vibrating cantilever beam and found to agree well.

Sodano *et al.* (2005) studied eddy current damping of a cantilever beam using the radial flux of a magnet rather than the flux perpendicular to the face. In the previous literature, eddy current damping has been studied in a configuration of two magnets with opposite poles facing, and a conductor moving through the gap between the magnets in a direction perpendicular to the field lines. While this is the most effective geometry as it maximizes the change in magnetic field experienced by the conductor, it is not always possible within geometric constraints. In this study, the authors used a single magnet with a cantilever beam vibrating towards and away from it. In this configuration, the component of the magnetic field in the same direction as the vibration of the beam does not contribute to the eddy current generation,

but the authors found that the radial component of the field was enough to increase the damping ratio by up to 150 times over the undamped case. They created a model to predict the eddy current damping and validated it experimentally using a permanent magnet and a cantilever beam with a copper plate attached to the end. The displacement of the beam was measured using a laser, allowing the logarithmic decrement to be calculated. The system was tested with various gaps ranging from 1-10 mm between the beam and the magnet. The experimentally measured damping ratio was found to decay from about 0.35 to 0.002 as the magnet gap increased. This configuration is of particular interest to the application of eddy current damping in machining as it is easiest to implement without affixing elements to modify the geometry of the workpiece.

Sodano (2005) describes three types of eddy current damper: passive, passive-active, and active. The passive damper is similar to the work described previously. A permanent magnet was affixed between 1 and 10 mm from a cantilever beam, with the beam motion in the same direction as the magnetic pole direction. The image method was used to predict the eddy current behaviour. The response of the beam was measured by giving it a consistent initial displacement and allowing it to vibrate freely. The beam was tested under various magnet gaps. The author also describes a configuration with two magnets with the same poles facing each other, and a cantilever beam vibrating in the gap between them. Additionally, rather than a cantilever beam, a beam fixed at either end to represent a vibration membrane is studied. In the passive-active damper, the position of the magnet is actively varied using a control system in order to maximize damping by minimizing the air gap between the conductor and the magnet. When applied to the same cantilever beam

setup described in the passive case above, it is found to reduce the settling time by 79% over the use of a stationary magnet. In the case of active damping, an electromagnet was used. This is beneficial in that it could be smaller and lighter than a permanent magnet, and it would allow the system to be turned off when not in use. The current to the electromagnet was changed constantly in a controlled way to change the magnetic flux and take advantage of the transformer EMF in addition to the motional EMF. The frequency of the force applied to the structure by the changing flux was found to be twice the frequency of the current applied to the electromagnet. The active system was found to be able to attenuate even high frequency modes, which is a limitation of the passive-active system due to the need to physically move the magnet. The settling time was comparable to the passive-active system.

Sodano *et al.* (2006b) used two magnets with the same poles facing each other to improve eddy current damping in a cantilever beam. The use of two magnets with the same poles facing each other displaces more of the field lines in a direction perpendicular to the motion of the conductor, allowing them to contribute more damping to the system (figure 2.7). The image method was used to predict the behaviour of the system. The maximum magnetic flux density was found to be doubled over the case with only one magnet, leading to a reduction in the frequency response function of the system of between 14 and 31 dB for the 2nd-4th modes of the system compared to the undamped case.

Sodano *et al.* (2006a) actively varied the position of the magnet compared to the vibrating conductor to improve damping. This addition of a control system improved the vibration in the second mode from 3 dB to -13 dB over a purely passive eddy current damper applied to the same system.

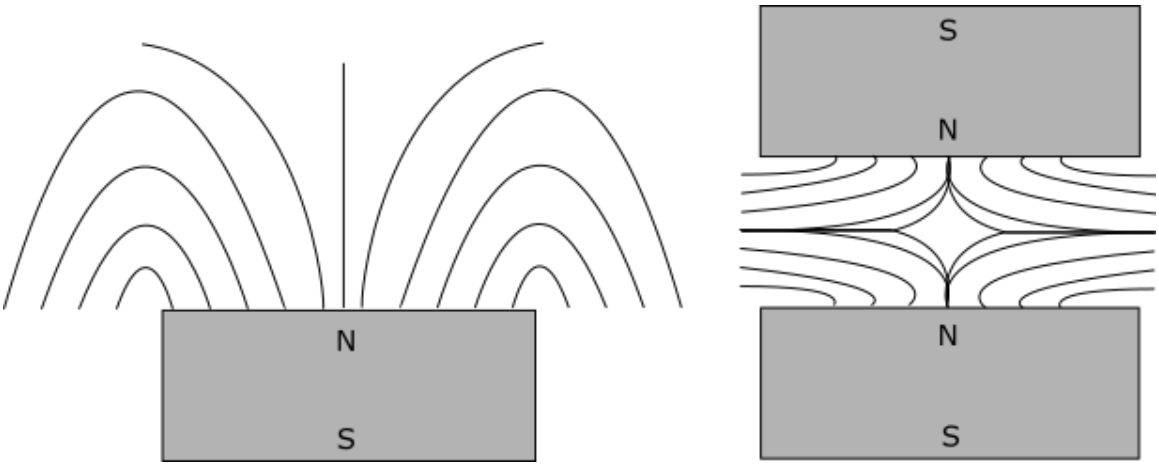

Figure 2.7: Magnetic field lines for one and two magnets, adapted from Sodano *et al.* (2006b)

Singh *et al.* (2012) used an electromagnet to initiate eddy current damping in a cantilever beam after vibration surpassed a threshold value. They found the damping ratio to be increased by 58.1% over the undamped case. It is unclear what benefit is gained from only initiating damping after a threshold vibration magnitude. The authors note that the use of electromagnets allows the magnetic flux to be varied, theoretically increasing the damping, however this does not appear to be attempted in this study.

2.4.3 Current Applications

A number of studies focus on specific applications of eddy current dampers. Sodano and Bae (2004) described three different areas of application of eddy currents: braking, rotating machinery, and dynamic systems. In braking systems, a conductive disk passes between two magnets arranged with opposite poles facing. This pole arrangement enables the maximum change in field strength experienced by the conductor

and thus generates the greatest braking force. The braking force has been found to be proportional to velocity, conductivity, the inverse of the air gap, and the square of the magnetic field strength. Eddy current use in braking has been studied using pendulums which swing between magnets. The pendulum is typically displaced and the settling time is measured. Active control of the magnetic field has also been applied to car braking systems to brake at an optimal level depending on road conditions. Several analytical models for braking have been developed using the image method.

The suppression of lateral vibrations in rotating machinery has also been identified as an application of eddy currents by Sodano and Bae (2004). Eddy currents have been found to be especially useful in cryogenic pumps due to the increased conductivity of the pump material at very low temperatures. Interesting results have been obtained using a conductor in a magnetic field mounted through ball bearings in a rotor. In this way, lateral vibrations can be reduced without slowing the rotation of the shaft and leading to instabilities at high speeds.

Finally, Sodano and Bae (2004) noted numerous applications of eddy currents in dynamic systems. Their ability to reduce vibration has been studied for application in road vehicle suspensions, solar sail arrays, launch vibrations in optical instruments for the Hubble telescope, industrial pipes, and suspension bridge ramps. Studies have noted that non-conductive components with conductive materials attached are also effective.

Sodano *et al.* (2006c) looked at eddy current vibration suppression of antenna surfaces in satellites and solar sails. Vibrations can be induced by guidance systems, space debris, and thermally induced by sunlight. Thin-film surfaces are used to minimize weight for launch, which results in an extremely flexible structure. The

authors used a thin membrane beam under tension to simulate the antenna surface. A 35.6 μm thick copper film was affixed in the center of the beam to act as a conductor, and a cylindrical permanent magnet was mounted 1 mm from the beam. The entire structure was attached to a shaker to induce vibrations in the membrane. The system was tested in laboratory conditions and in a vacuum. In laboratory conditions, the first bending mode vibration amplitude was reduced by 13.7 dB compared to the undamped case, while in vacuum conditions, the amplitude was reduced by 31.06 dB.

2.5 Eddy Current Damping in Machining

Recently, several studies on the application of eddy current damping to reduce machining vibrations have been conducted. Yang *et al.* (2015b) attached to the workpiece an aluminum bar with a magnet on the end. The bar vibrated in an aluminum tube fixed with its axis perpendicular to the surface of the workpiece, as seen in figure 2.8. Since the eddy current conductor was not restricted by the workpiece material, it is unclear why aluminum was used rather than a more conductive material. The thin-walled workpiece was excited with an electromagnetic shaker to simulate machining vibrations. The response of the system was measured using an accelerometer, and CutPro (Manufacturing Automation Laboratories Inc, 2011) was used to analyze the results. Machining tests were then carried out to ensure agreement with the electromagnetic shaker-induced response. The authors saw an increase in the damping ratio for the first mode from 0.41 to 1.47, however the stability lobes appear to show a decrease in the limiting depth of cut with the added damping.

Yang *et al.* (2015a) also developed a small eddy current damper which could be glued to a workpiece. The damper consisted of a permanent magnet mounted

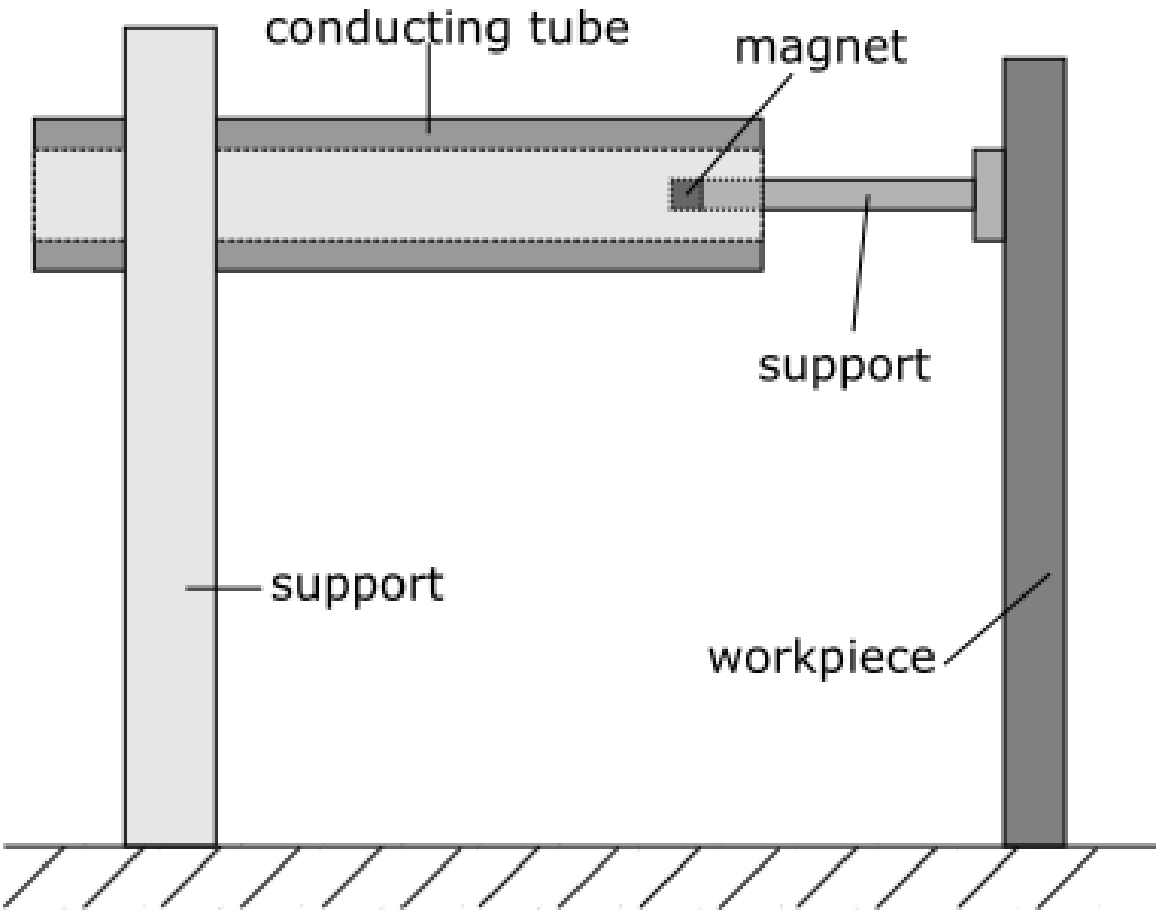

Figure 2.8: Fixture for applying eddy current damping, adapted from Yang *et al.* (2015b)

on a rod with springs on either side, and a conducting tube around it (figure 2.9). They mounted the damper to a cantilever beam and tested the response using an impact hammer. A laser vibrometer was used to measure vibrations. The device was affixed during different tests at various locations: at one third of the length of the beam from the fixed end, at two thirds, and at the tip of the beam. The impact occurred close to the fixed end of the beam, and the vibration was measured at the free end. Unsurprisingly, the greatest damping was found to occur when the damper was attached at the tip of the beam, although this was found to lower the natural frequency significantly due to the added mass. Despite one of the most lauded merits of eddy current damping being its non-contact properties, this study does not take advantage of that merit. The authors found the damping ratio to increase from 0.14 in the undamped system to 0.64 when the damper was mounted at the tip of the beam. Machining tests were then carried out on a thin-walled box. The addition of the damper saw the damping ratio increase from 0.07 to 0.34 in the first mode, 0.26 to 0.42 in the second mode, and 0.08 to 0.24 in the third mode. The authors also observed an improvement in surface finish with the use of the eddy current damper. The R_a value in μm) decreased from 0.49 to 0.15 at 400 mm/min, from 2.27 to 0.43 at 800 mm/min, and from 4.76 to 0.53 at 1200 mm/min. Tests were also conducted at various depths of cut and spindle speeds.

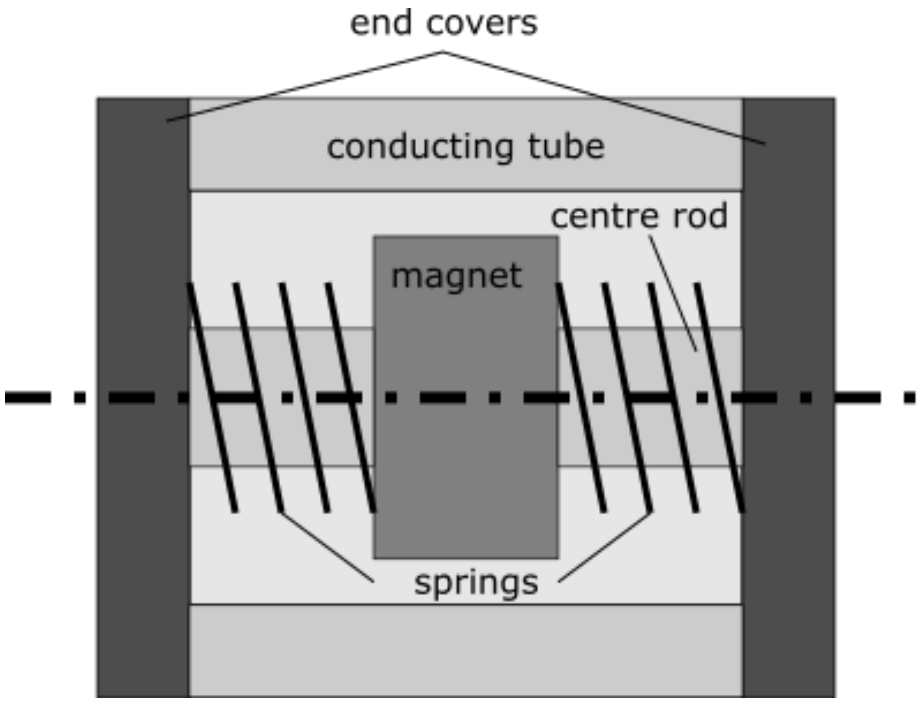

Figure 2.9: External eddy current damper design, adapted from Yang *et al.* (2015a)

Chapter 3

Experimental Design

3.1 C-Channel

To validate the benefit of applying eddy current damping to machining, a simple test was carried out. A workpiece was mounted in the centre of a long section of 6061-T6 aluminum c-channel using bolts. The c-channel was four inches wide, two inches high, and had wall thickness of a quarter of an inch. The c-channel was fixed at both ends and free to vibrate in the middle. Magnets were clamped a small distance away from either side of each vertical wall of the c-channel. The magnet location was in the middle of the length of the c-channel. The workpiece was then machined with an indexable end mill. The experimental setup is shown in figure 3.1.

As the machining was performed, the c-channel vibrated in the vertical direction. This resulted in the direction of motion of the aluminum being perpendicular to the field lines connecting the magnets (figure 3.2). This is the configuration which has the potential to provide the greatest damping, which is why it was desirable to test it before proceeding with more realistic machining configurations. If magnetic damping

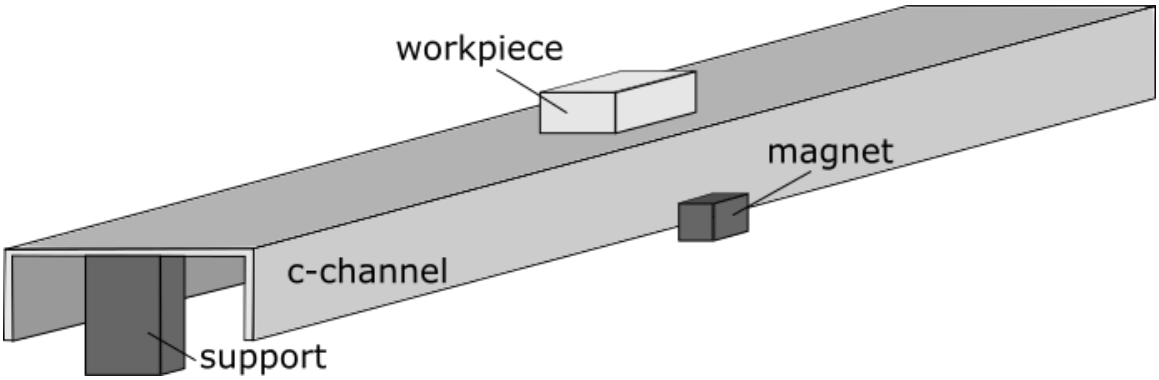

Figure 3.1: Experimental c-channel setup

did not provide a noticeable benefit in this case, it would be unlikely to do so in any machining situation.

It was expected that this vibration of the c-channel in the magnetic field would add damping to the system. The eddy currents would dissipate energy through heat and result in a more stable system. A machining pass was taken on the setup both with and without the magnets in place. Both tests used the same machining parameters. A better surface finish was expected when the magnets were in place adding damping to the system.

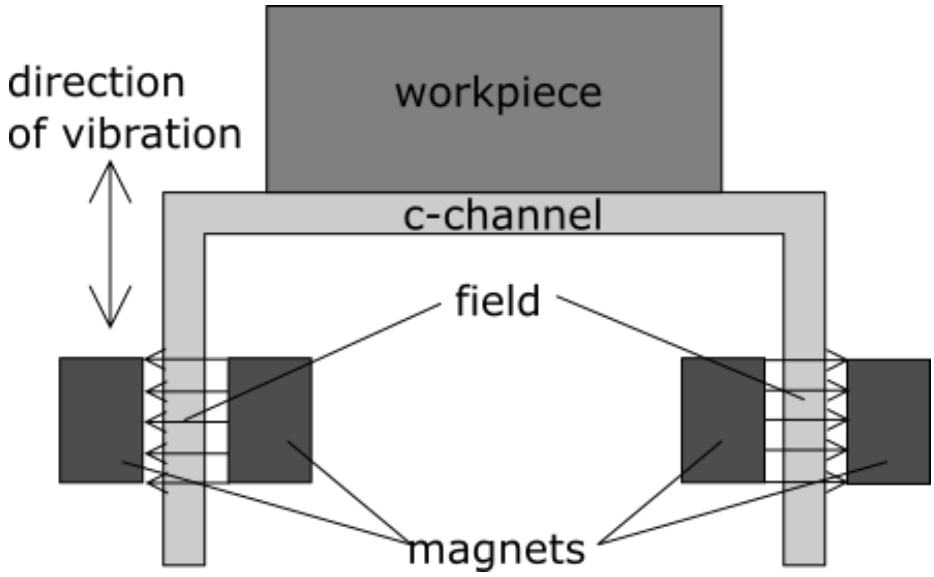

Figure 3.2: Magnetic field lines in c-channel testing

3.2 MATLAB Model

3.2.1 X and Y Directions

A numerical simulation of machining forces was carried out in MATLAB in order to predict the effects of eddy current damping on machining stability.

Cutting forces in milling are typically assumed to be proportional to the uncut chip thickness by a cutting force coefficient (K) which depends on the workpiece material and is usually determined through cutting tests. At a given rotational position of the tool, the tangential cutting force on an axial increment of a single tooth of the tool is given by

$$F_t = K_t \cdot \delta b \cdot h \tag{3.1}$$

where K_t is the tangential cutting force coefficient for the material, δb is the thickness of the axial segment being examined, and h is the uncut chip thickness.

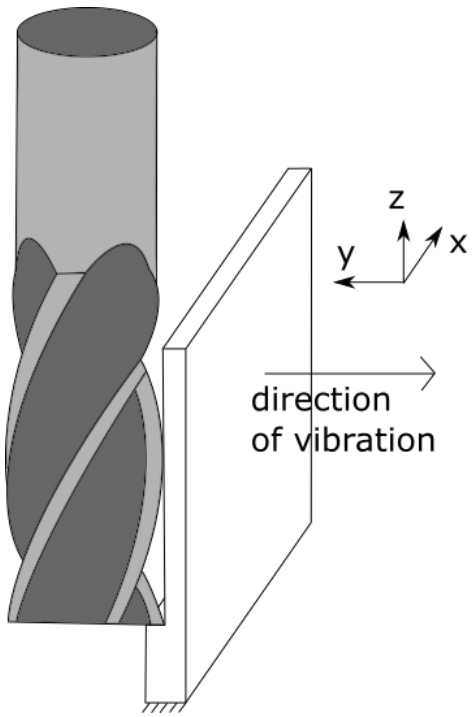

Figure 3.3: Milling system being considered in the x and y direction MATLAB simulation

Similarly, the normal force can be expressed as

$$F_n = K_n \cdot \delta b \cdot h \tag{3.2}$$

where K_n is the normal cutting force coefficient.

The cutting thickness is calculated based on the programmed feed rate per tooth, the deflection of the tool caused by vibrations, and the waviness left on the surface by the previous tooth pass:

$$h = feed \cdot \sin\theta + d_x \sin\theta + d_y \cos\theta - d_{x,previous} \sin\theta - d_{y,previous} \cos\theta \tag{3.3}$$

where θ is the angle of the tooth with respect to the positive y-axis. The negative values in the terms for deflection from the previous tooth pass represent the fact that a positive displacement on the previous tooth will have resulted in more material having been removed, leading to a smaller uncut chip thickness for the current tooth.

These forces can be transformed into X and Y coordinates based on the angle of the tooth at the cutter angle:

$$F_x = F_t \cos\theta + F_n \sin\theta \tag{3.4}$$

$$F_y = F_t \sin\theta - F_n \cos\theta \tag{3.5}$$

The forces on that tooth for each axial segment are summed after checking to ensure the axial segment is engaged in the workpiece material based on the cutting depth and helix angle. The process is repeated for all teeth which are currently cutting, and the results are summed. This gives the total force on the tool, in x and

y, for a given rotation angle.

The forces on the tool along with the velocity and deflection from the previous cutter rotation angle increment are used to determine the acceleration in x and y as follows:

$$a_x = \frac{F_x - c_x \cdot v_x - k_x \cdot d_x}{m} \tag{3.6}$$

$$a_y = \frac{F_y - c_y \cdot v_y - k_y \cdot d_y}{m} \tag{3.7}$$

where c is the damping coefficient and k is the stiffness. Since "machining chatter is always caused by the dominant mode of the most flexible component" in a milling system (Wang, 2011), for simulation of a compliant workpiece, the tool can be assumed to be rigid. The value of k will therefore represent the stiffness of the workpiece only. Since the workpiece does not have the same characteristics in the x and y directions, the stiffnesses in each of these directions will have to be assessed separately. The value of c is normally dependent on the inherent process damping. In this simulation, the applied magnetic damping will also be considered. Again, this value will differ for each direction. Discussion of its determination will be presented in a subsequent section.

The velocity and deflection for the current cutter rotation angle increment can be determined by multiplying the acceleration and velocity by the time increment and

adding to the present value as follows:

$$v_{x,current} = v_{x,previous} + a_x \delta t \tag{3.8}$$

$$v_{y,current} = v_{y,previous} + a_y \delta t \tag{3.9}$$

$$d_{x,current} = d_{x,previous} + v_x \delta t \tag{3.10}$$

$$d_{y,current} = d_{y,previous} + v_y \delta t \tag{3.11}$$

The rotation angle of the cutter is then incremented and the process is repeated. Since the cutting forces and therefore the behaviour of the system depend on the surface left by the previous tooth, several rotations of the cutter are simulated. In a stable cutting scenario, the amplitude of the periodic forces will settle after several revolutions. If unstable chatter vibrations are occurring, the amplitude of the periodic forces will grow, limited by the instability of the tooth jumping out of the cut. Chatter can therefore be assessed by observing whether the amplitude of the cutting force increases or decreases.

3.2.2 Z Direction

Since the cutting edge of the tool has a helix angle, any force applied by the tool on the workpiece will have a component in the z direction. In a peripheral milling operation, both the tool and workpiece tend to have high stiffness in the z direction compared to the x and y directions, so the z direction is typically ignored in machining simulation. In the case of end milling a minimally-supported thin plate however, the greatest compliance belongs to the workpiece in the z direction.

While this compliance can be significantly decreased by greater workpiece support,

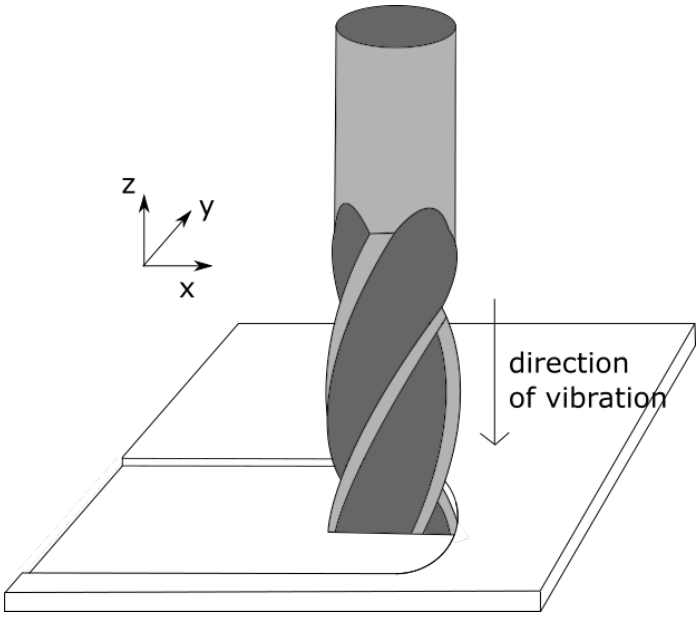

Figure 3.4: Milling system being considered in the z direction MATLAB simulation

this is undesirable in many situations as it induces fixturing stress into the workpiece. This stress relaxes when the workpiece is unclamped, causing deformation of the workpiece. The deformation of such a compliant workpiece can easily move it out of the flatness tolerance. Deformation of thin plate workpieces is a much greater danger than thicker workpieces due to their high compliance, and for this reason, it is even more important not to clamp them excessively.

Avoiding excessive clamping and allowing this high z-direction compliance during machining necessitates the consideration of z direction behaviour in the machining simulation. In order to accomplish this, a simulation was constructed similarly to the above x and y direction case, but the behaviour of the system in the z direction was also taken into account. The same force equations were used to calculate the feed and tangential forces. The z direction force was based on these forces and the helix

angle of the tool as follows:

$$F_z = F_t \sin \beta \tag{3.12}$$

where β is the helix angle of the tool.

In addition to this, vibration in the z direction will cause the depth of cut to change. The depth of cut must be noted at each rotation angle increment and used in the following increment to calculate the cutting forces. As the workpiece vibration causes it to move towards the tool and the depth of cut increases, the cutting forces will also increase.

3.3 Determining the Damping Coefficient

Zuo (2005) describes the damping coefficient due to eddy currents as

$$C = C_0 B^2 t A \sigma \tag{3.13}$$

where B is the magnetic flux density in Tesla, t is the thickness of conductor plate in m, A is the area of the conductor in the magnetic field in m^2, σ is the electrical conductivity of the conductor in $(\Omega m)^{-1}$, and C_0 is a dimensionless coefficient related to shape and size, which typically falls between 0.25 and 0.4 for a relatively large conducting plate. Nagaya *et al.* (1984) note that the dimensionless coefficient C_0 is greater for a smaller gap between the magnet and the conductor and for a larger conductor.

This value can be challenging to compute due to the non-uniformity of the magnetic field and the difficulty in obtaining the dimensionless coefficient, C_0. Nagaya

Table 3.1: Dimensionless damping coefficient for a rectangular conductor for $a_1/a_2 = 0.3$, $t_m/a_2 = 0.6$, and $a_2/b = 0.3$ (Nagaya *et al.*, 1984).

		l/b				
		0.5	1.0	1.5	2.0	4.0
	0.1	0.8081	1.0950	1.1110	1.1119	1.1128
	0.2	0.4107	0.6313	0.6454	0.6519	0.6581
G/a_2	0.3	0.2413	0.4046	0.4172	0.4222	0.4264
	0.4	0.1593	0.2770	0.2881	0.2917	0.2944
	0.5	0.1148	0.1979	0.2075	0.2102	0.2117

et al. (1984) determined the dimensionless damping coefficient for a number of different configurations. An example of these values for a rectangular conductor and an annular magnet where $a_1/a_2 = 0.3$, $t_m/a_2 = 0.6$, and $a_2/b = 0.3$ can be seen in table 3.1. The table shows damping coefficients for a variety of conductor length to width ratios and air gap to magnet radius ratios. In the table, l and b are the dimensions of the rectangle, a_1 and a_2 are the inner and outer radii of the annular magnet, t_m is the thickness of the magnet, and G is the air gap between the magnet and conductor. It can be seen that the dimensionless damping coefficient, and therefore the amount of damping is very sensitive to the size of the air gap between the magnet and conductor relative to the size of the magnet. The values are somewhat less sensitive to the relative dimensions of the rectangular conductor. Even the numerous values in this table only pertain to particular magnet and conductor geometry and relative magnet and conductor dimensions. These values, while computed analytically by Nagaya *et al.* (1984), are reasonably complicated to obtain.

The damping value can more easily be obtained experimentally using a method employed in much of the literature. This method applies particularly well to the use of eddy current damping for vibrating systems. The conductor, placed near a stationary magnet, is given an initial consistent displacement and allowed to vibrate freely, with

these vibrations measured using an accelerometer. The test can be repeated without a magnet present to allow internal damping of the structure to be neglected in the final eddy current damping coefficient. This method is limited in that it has the potential for the mass of the accelerometer to affect the behaviour of the system. However, since only the damping coefficient and not the damping ratio is important here, this effect is not problematic.

To more easily determine the damping coefficient, it is desirable to perform testing on a simplified system such as a cantilever beam. It is necessary to ensure that the damping coefficient obtained in this way will be valid for a machining case. The parameters that influence the damping coefficient can be seen in equation 3.13. The magnetic flux density is dependent on the strength and geometry of the magnet. As long as the same magnet is used in the same way, this value will remain the same. The area of the conductor in the magnetic field will remain the same as long as the conductor is either the same shape and size, or sufficiently large. The conductivity of the material will be unchanged as long as the same material is used for both tests.

The dimensionless coefficient, C_0 has the greatest potential for change between the cantilever beam and machining tests. It depends on the geometry of the magnet and the gap between the magnet and conductor, which can easily be maintained. It also depends on the geometry of the plate, as seen in table 3.1. However, these values are for a relatively small plate compared to the size of the magnet ($a_2/b = 0.3$). Zuo (2005) notes that for a uniform magnetic field and an infinite conducting plate, the value of C_0 is 1. It follows from this that for a sufficiently large conducting plate compared to the magnet size, differences in the size of the plate will have negligible effect on the damping coefficient. For a conductor of the same size and shape the

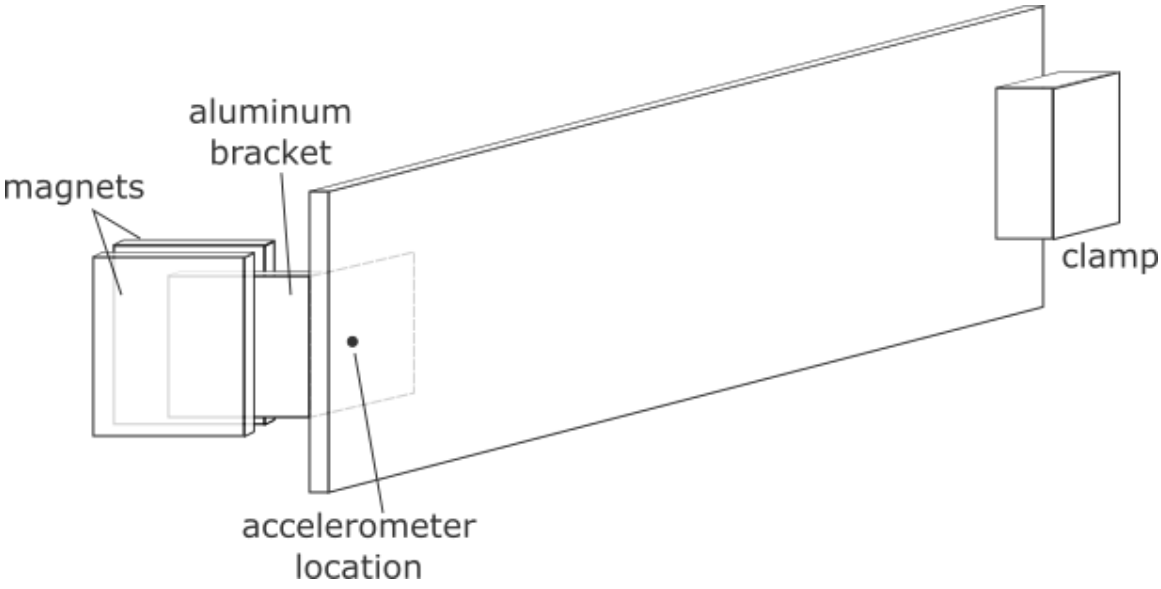

Figure 3.5: Vibration testing setup for the third magnet configuration

values will be the same.

In order to test the damping coefficient in this way, a thin plate was fixed at one end. An L bracket was adhered to the back of the cantilever beam at the free end and arranged to vibrate in a transverse direction in a gap between two magnets. The L bracket was two inches in length, and its profile was two inches high by one inch wide by one eighth of an inch in thickness. The magnets both had dimensions of two and a quarter inches wide by one and five eighths inches high by one quarter inch thick. This configuration takes advantage of the preferential vibration direction with respect to the magnetic field. This setup is shown in figure 3.5.

Due to the thickness of the plate and the difficulty in giving it a consistent initial offset, impact testing was used instead. A rubber mallet was used to tap the free end of the plate, inducing vibration. An accelerometer affixed to the end of the plate was used to measure vibrations. Details of the accelerometer are listed in table 3.2. From

Table 3.2: Accelerometer details

Manufacturer	Kistler
Type	8640A5
Measuring Range	±5 g
Sensitivity	990 mV/g
Transverse Sensitivity	3.0%
Resonant Frequency	17.0 kHz
Temperature	-40 ... 55 °C

the decay of the vibrations, the damping coefficient could be determined.

3.4 Thin Plate

To experimentally validate the stability and surface finish improvement on a realistic machining scenario, a trial was conducted on a thin plate. A 6061-T6 aluminum plate with dimensions 10 inches by 10 inches by 0.125 inches was mounted on a force dynamometer. The properties of the dynamometer are shown in table 3.3. The plate was mounted using bolts whose centers formed a square with side length 210 mm. An L bracket was welded to the underside of the plate and allowed to move freely between two magnets, mounted to the table underneath the plate. The experimental setup is shown in figure 3.6.

A machining pass was taken across the surface of the aluminum plate. The tool

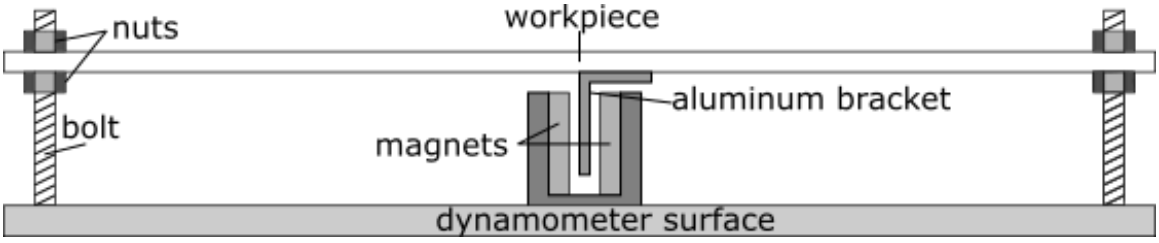

Figure 3.6: Experimental setup for eddy current damping testing on thin plate machining

Table 3.3: Dynamometer details

Manufacturer	Kistler
Type	9255B
X and Y Range	-20 to 20 kN
Z Range	-10 to 40 kN
X and Y Sensitivity	-8 pC/N
Z Sensitivity	-3.7 pC/N
Linearity	$\leq \pm 1\%$ FSO
Hysteresis	$\leq \pm 0.5\%$ FSO
Cross Talk	$\leq \pm 2\%$
Natural Frequency	3 kHz
Temperature	0 ... 70 °C

Table 3.4: Cutting parameters used for the flat plate test

Cutting Speed	2500 ft/min
Chip Load Per Tooth	0.003 in
Cutter Diameter	3 in
Spindle Speed	3200 RPM
Feed Rate	50 in/min
Axial Depth of Cut	0.005 in

used was a three-inch diameter five-tooth indexable cutter with sharp inserts for machining aluminum. Cutting parameters were selected based on standard machining practices and are listed in table 3.4. The forces from the dynamometer were collected during machining, and the surface finish of the part was measured after machining. The test was repeated without magnets in order to allow the increase in damping and the improvement in part quality to be quantified.

Chapter 4

Results and Analysis

4.1 C-Channel

During machining of the c-channel configuration with no magnetic damping, considerable vibration of the workpiece in the vertical direction was observed. Significantly less vibration could be heard when machining was conducted on an identical setup but with magnetic damping in place. These qualitative observations were supported by the surface finish which could be observed on the parts.

The roughness of the surfaces was measured using a Zygo white light interferometer. Eight measurement locations were selected on each workpiece. The measurement locations are shown in figure 4.2. The roughness measurements can be seen in table 4.1. Images of the surface profile generated by the interferometer can be seen in figure 4.3.

A photo of the two surfaces can be seen in figure 4.1. It is interesting to note that the ridges formed by passing teeth can be seen in the image for the damped part. For the undamped part, the local surface may be smoother, but it exhibits a large drop

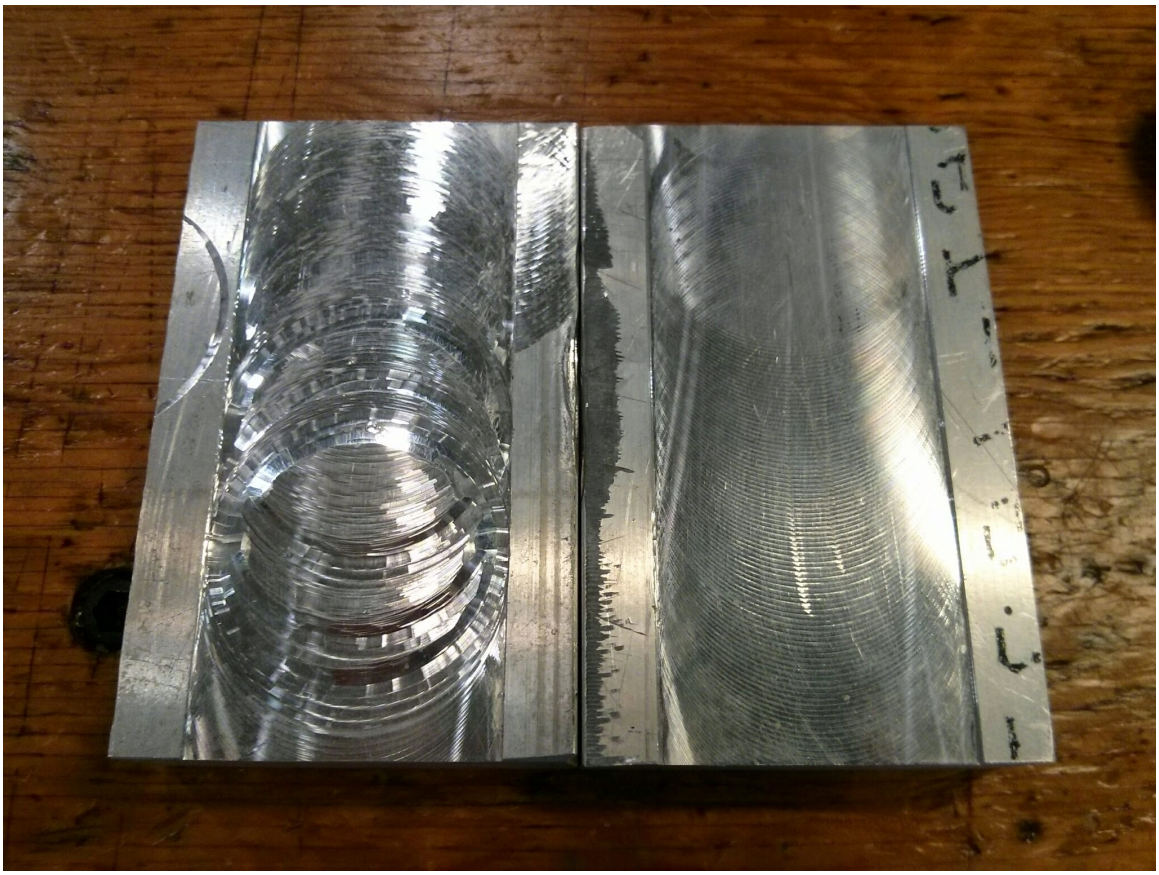

Figure 4.1: Surface finish left on parts after machining without (left) and with (right) magnetic damping

Table 4.1: Interferometer roughness measurements on damped and undamped c-channel-mounted workpieces

Location	Undamped Part R_a (μm)	Damped Part R_a (μm)
A	5.579	0.793
B	8.224	0.997
C	14.853	1.745
D	14.198	1.999
E	8.708	1.473
F	9.184	1.887
G	24.465	1.269
H	19.219	1.389
Average	13.054	1.444
Standard Deviation	6.390	0.423

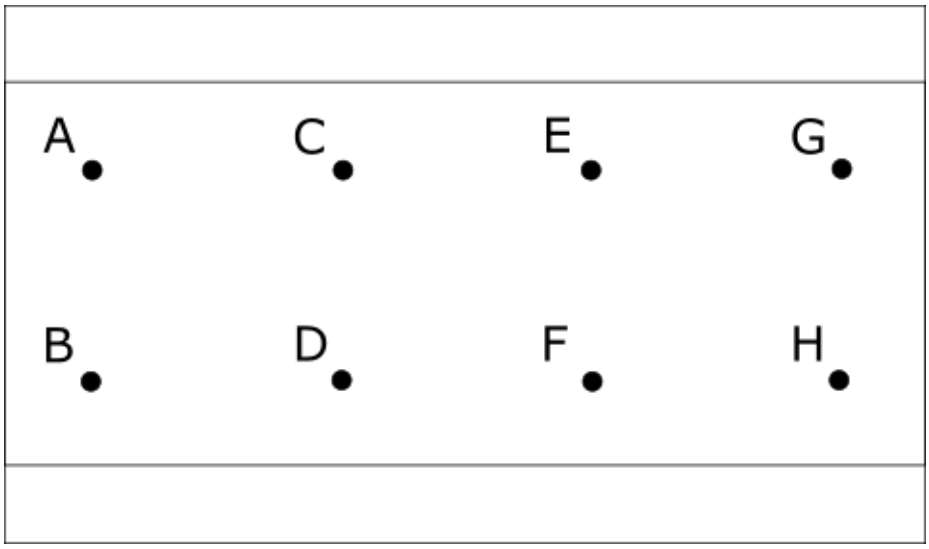

Figure 4.2: Roughness measurement locations on workpiece from c-channel test; the rows are located 15mm above and below the centre of the machined channel in the vertical direction; the outer columns are located 15 mm from the left and right edges of the part, and the middle two columns are evenly spaced between the outer columns

in the middle due to excessive vibration of the tool.

It can be seen from the interferometer measurements that a considerable improvement in surface finish was achieved through the use of eddy current damping, with an average undamped R_a value over eight times that of the damped value. In addition to the decrease in roughness, the standard deviation for both sets of measurements indicates that the damped part also has a more consistent surface, which is a desirable quality for machined parts.

It is also important to note that the measurements are limited in terms of scale. The interferometer is restricted in the change in height it can accurately measure, and in the size of frame it can view. The image of the undamped workpieces clearly shows that the large variations in surface roughness are also relatively large in the surface plane directions. The undamped part shows not only a poor surface finish

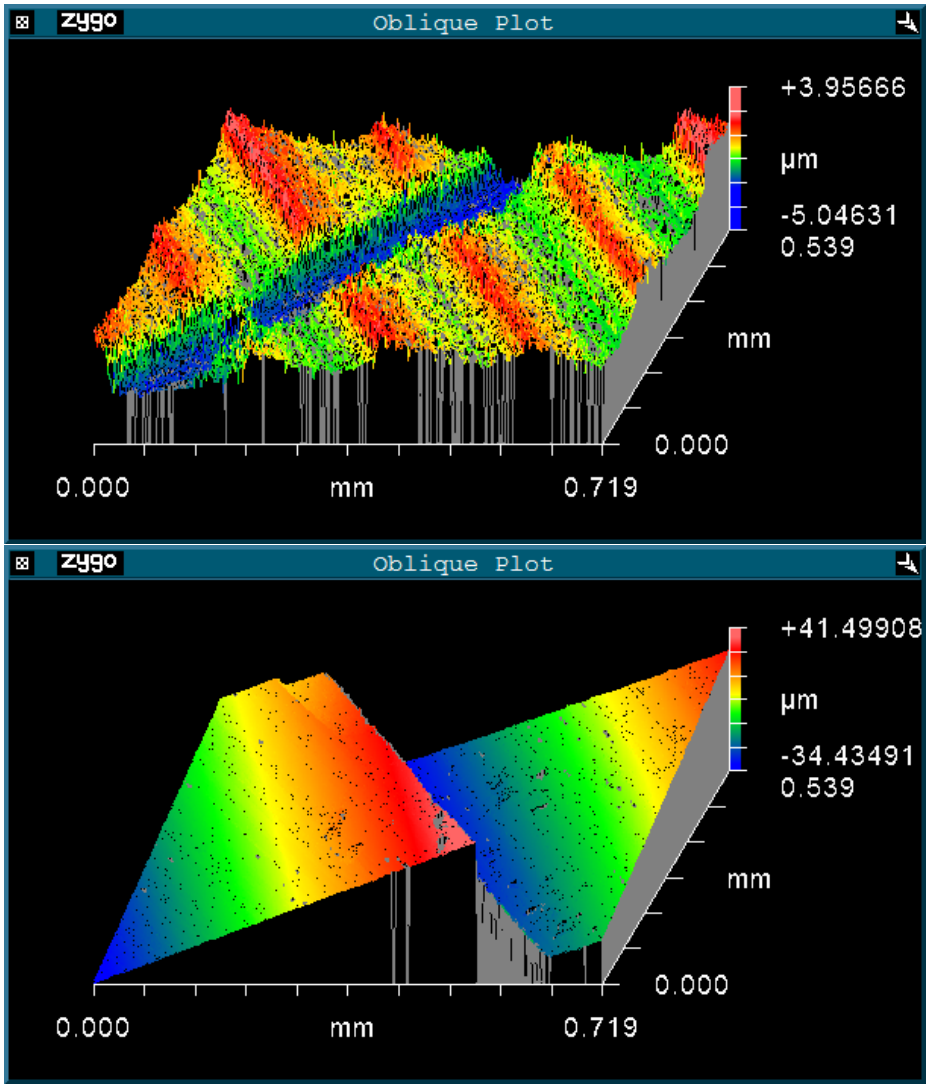

Figure 4.3: Surface profile captured by the interferometer for location A on the damped part (top) and location D on the undamped part (bottom)

on a micro scale, as measured by the interferometer, but also poor form on a much larger scale.

4.2 Determining the Damping Coefficient

Figure 4.4 shows an example of an acceleration signal collected during tap testing of the undamped cantilever beam. From this data, the damping ratio and subsequently the damping coefficient can be calculated:

$$\delta = \frac{1}{m} \ln \frac{x_1}{x_{m+1}} \tag{4.1}$$

$$\zeta = \frac{\delta}{\sqrt{(2\pi)^2 + \delta^2}} \tag{4.2}$$

$$c = 2\zeta\sqrt{mk} \tag{4.3}$$

The effective mass of a cantilever beam is known to be

$$m_{eq} = 0.23m + M \tag{4.4}$$

and the effective stiffness is

$$k_{eq} = \frac{3EI}{l^3} \tag{4.5}$$

The moment of inertia depends on the cross-sectional dimensions of the beam:

$$I = \frac{1}{12} w t^3 \tag{4.6}$$

where w is the width of the beam and t is the thickness.

Ten trials were conducted for both the undamped and the magnetically damped

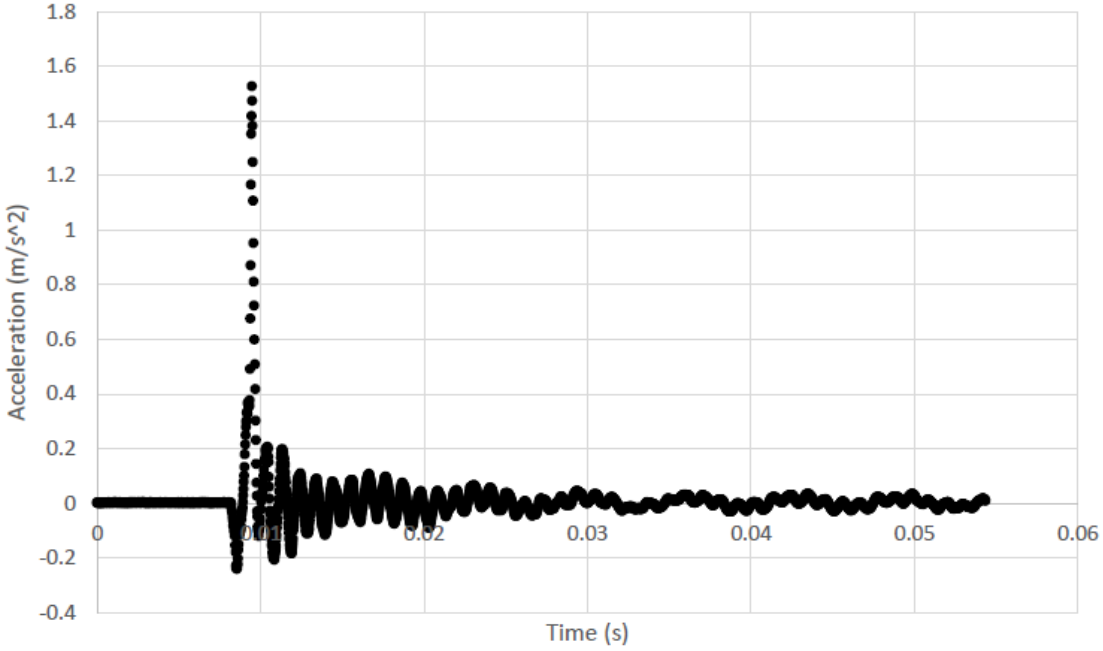

Figure 4.4: Accelerometer data from impact testing of the undamped cantilever beam

cases. The results of the trials are listed in table 4.2

Images of the test setup can be seen in figures 4.5 and 4.6

It can be seen that the addition of magnetic damping through the L bracket and magnet setup noticeably increased the logarithmic decrement in the measured acceleration of the cantilever beam.

The average value of logarithmic decrement from the ten L bracket trials was used to calculate the damping coefficient. The properties of the aluminum cantilever beam used for the damping coefficient calculations are listed in table 4.3.

The calculated values are listed in table 4.4.

Table 4.2: Logarithmic decrement values from ten impact testing trials

	Logarithmic Decrement	
Trial	Undamped	L Bracket
1	0.232	0.240
2	0.135	0.264
3	0.179	0.226
4	0.164	0.315
5	0.278	0.173
6	0.172	0.254
7	0.214	0.157
8	0.177	0.278
9	0.174	0.191
10	0.096	0.263
Average	0.182	0.236

Figure 4.5: Images of the undamped impact test setup

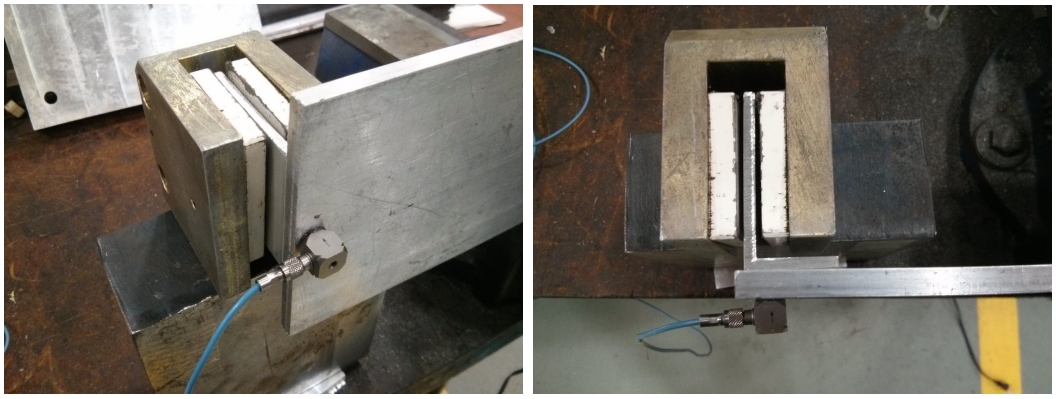

Figure 4.6: Images of the damped impact test setup

Table 4.3: Physical properties of the aluminum cantilever beam

Density	2.7 g/cm^3
Length	167 mm
Width	101 mm
Thickness	6.35 mm
Young's Modulus	68.9 GPa

Table 4.4: Calculated properties of the aluminum cantilever beam

Property	Damped	Undamped
Moment of Inertia (I)	2.16×10^4 mm^4	2.16×10^4 mm^4
Effective Stiffness (k_{eq})	95.6 N/mm	95.6 N/mm
Effective Mass (m_{eq})	98.3 g	66.5 g
Logarithmic Decrement (δ)	0.236	0.182
Damping Ratio (ζ)	0.0375	0.0290
Damping Coefficient (c)	7.27	4.62

4.3 MATLAB Model

In order to simulate the cutting conditions for the flat plate cutting test, it is necessary to determine the stiffness and effective mass of the system. For simplicity, the plate will be modelled as a simply supported beam with a load in the middle to determine the Z direction parameters. The system is assumed to be comparatively stiff enough in the X and Y directions as to be considered rigid.

The Z direction simulation was conducted using cutting conditions from the flat plat experiment. The cutting parameters and system properties used for the simulation are shown in table 4.5.

The simulation parameters are shown in table 4.6.

Chatter was assessed by observing the trend in the Z direction deflection over 100 rotations of the tool. A general increase in peak deflection as seen in figure 4.7 was indicative of unstable cutting, whereas a decrease to eventual steady conditions as seen in figure 4.8 was indicative of stable cutting.

Additionally, examining the force data (figure), two frequencies can be observed: a higher frequency corresponding to the tooth passing frequency, and a lower frequency corresponding to the dynamic characteristics of the system.

Although the simulations represent general trends about the behaviour of the undamped and damped system, it is difficult to simulate the complexities of this cutting scenario. First, since the depth of cut is very small, ploughing has a greater relative effect than in scenarios with larger depths of cut. Additionally, vibrations in a flat plate are complex and multi-modal, and this is difficult to capture in a simple simulation. A more detailed model would better capture the dynamics of the system. Finally, simulations capturing X and Y direction forces appear more frequently in

Table 4.5: Z Direction MATLAB Model Cutting and System Parameters

Number of Teeth	5
Cutter Diameter	3 inches
Tool Angular Speed	3200 RPM
Depth of Cut	0.005 inches
Helix Angle	30°
Entry Angle	0°
Exit Angle	180°
Tangential Cutting Force Coefficient	∼650 N/mm^2(Hamade *et al.*, 2006)
Normal Cutting Force Coefficient	∼200 N/mm^2(Hamade *et al.*, 2006)
Feed Rate per Tooth	0.003 inches
Z Direction Stiffness	137 N/mm
Z Direction Effective Mass	276.5 g
Z Direction Damping Ratio	0.0375

Table 4.6: Z Direction MATLAB Model Simulation Parameters

Axial Step Size	0.001 mm
Number of Angular Steps	10000
Number of Tool Rotations	100

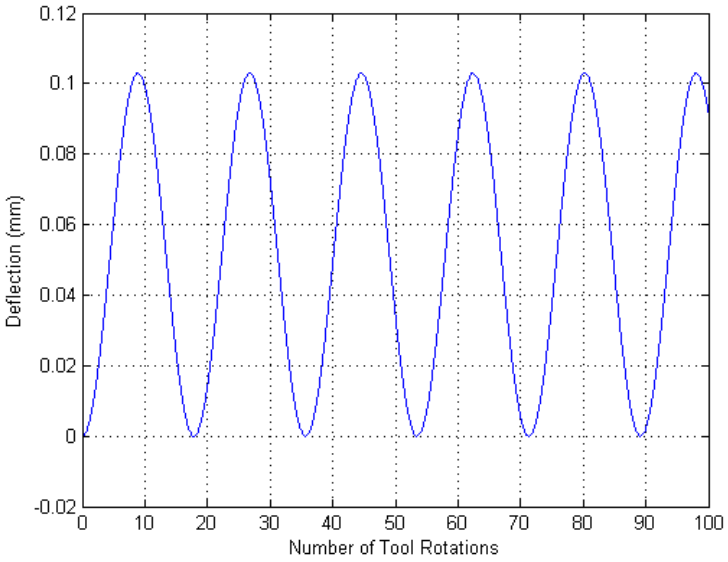

Figure 4.7: Z direction deflection over 100 rotations of the tool indicative of unstable cutting conditions

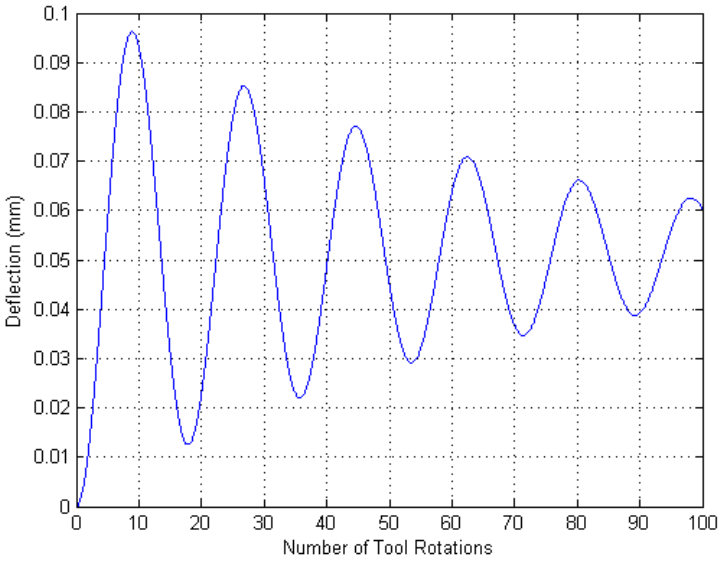

Figure 4.8: Z direction deflection over 100 rotations of the tool indicative of stable cutting conditions

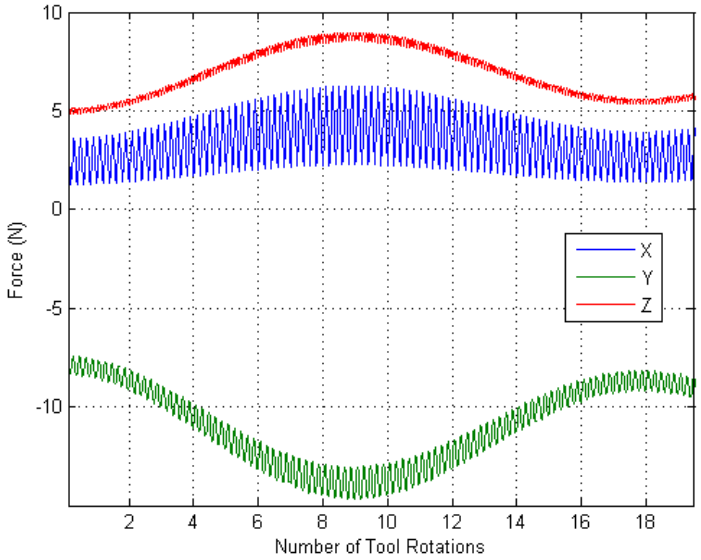

Figure 4.9: Simulated forces showing tooth passing frequency and natural frequency of the system

the literature. The Z direction forces depend more strongly on complicated factors such as tool wear and edge radius. Still, even a simple simulation can provide useful information about the behaviour of the system.

4.4 Thin Plate

Photographs of the test setup for the machining of the thin plate is shown in figure 4.10.

Figure 4.11 shows photographs of the machined surfaces of the thin plate test both with and without eddy current damping. While the damped test was not sufficiently damped to entirely eliminate chatter, visual inspection clearly shows that the amplitude of vibrations is considerably higher for the case without magnetic damping.

4.4.1 Machining Forces

Graphs of the forces collected by the dynamometer during machining are shown in figures 4.12 and 4.13. It can be seen that the addition of eddy current damping and its suppression of excessive vibration results in an order of magnitude decrease in the forces in all directions. The peak on the FFT occurs close to the tooth passing frequency as expected and has approximately twice the magnitude in the undamped case.

Zooming in on a smaller time increment of the forces as in figures 4.14 and 4.15 shows their periodic nature. While it is difficult to observe an increase in the magnitude of the forces on this scale, it can be seen that the forces for the undamped case are less smooth and regular, particularly in the z direction. The 0.06 seconds of

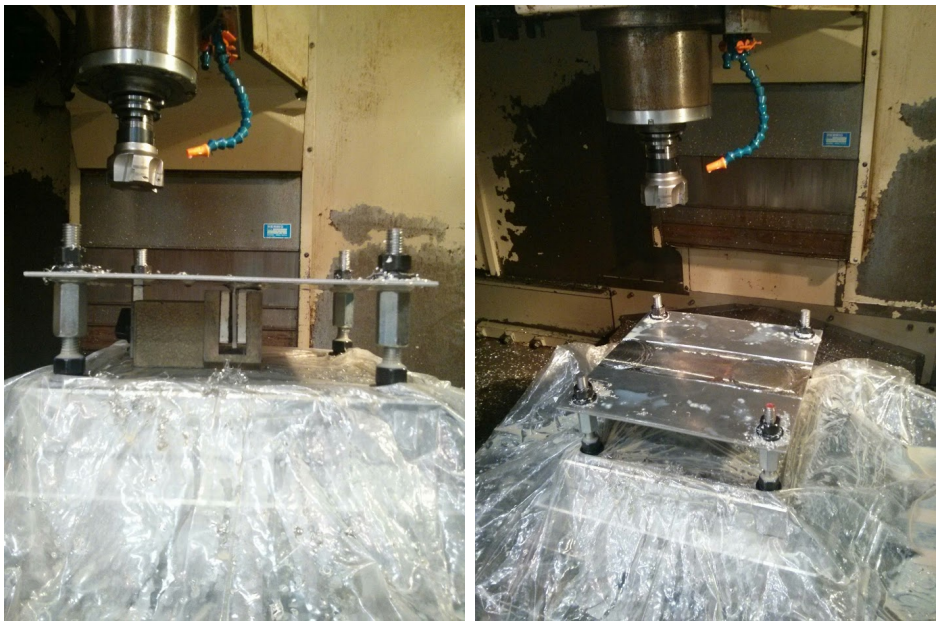

Figure 4.10: Thin plate test setup photographs

data shown in the figures represents 3.2 revolutions of the tool, or 16 teeth passing through the part. The dominant frequency shown in the graph is therefore the tooth passing frequency, which is to be expected based on the Fast Fourier Transform.

4.4.2 Surface Finish

The machined plates were visually divided into four rows of five columns, as seen in figure 4.16. Surface roughness measurements were conducted on a white light interferometer in each of the sections. An attempt was made to select a measurement location within each section that was representative of the surface finish in the section as a whole. The measurements for the damped and undamped workpieces are listed in table 4.7.

Examples of the surface profile measured on the interferometer can be seen in figure 4.17.

Figure 4.11: Images of the machined thin plate without magnetic damping (top) and with magnetic damping (bottom)

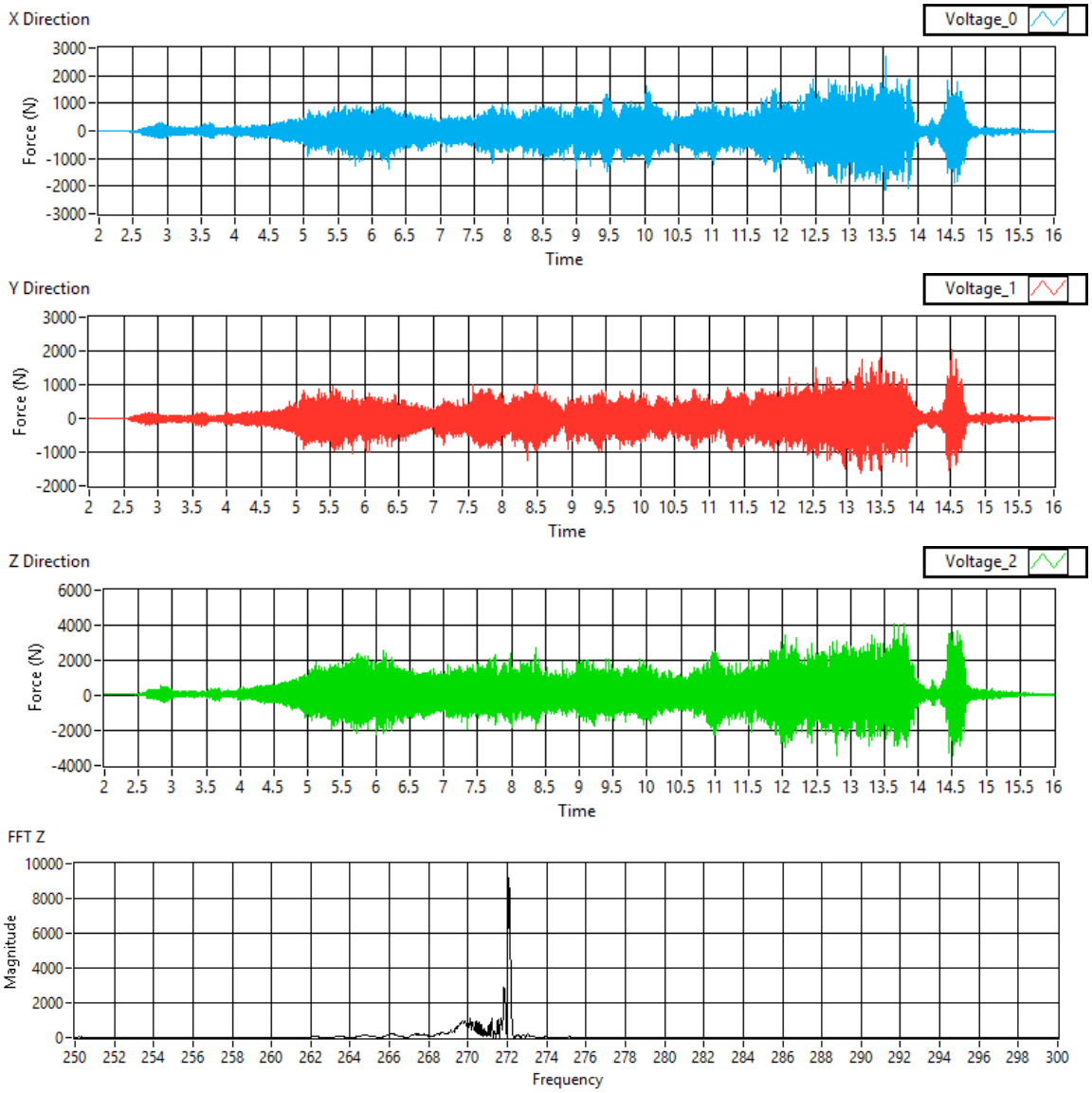

Figure 4.12: Measured machining forces in the X Y and Z directions during undamped machining of the flat plate, along with the Fast Fourier Transform of the Z direction force

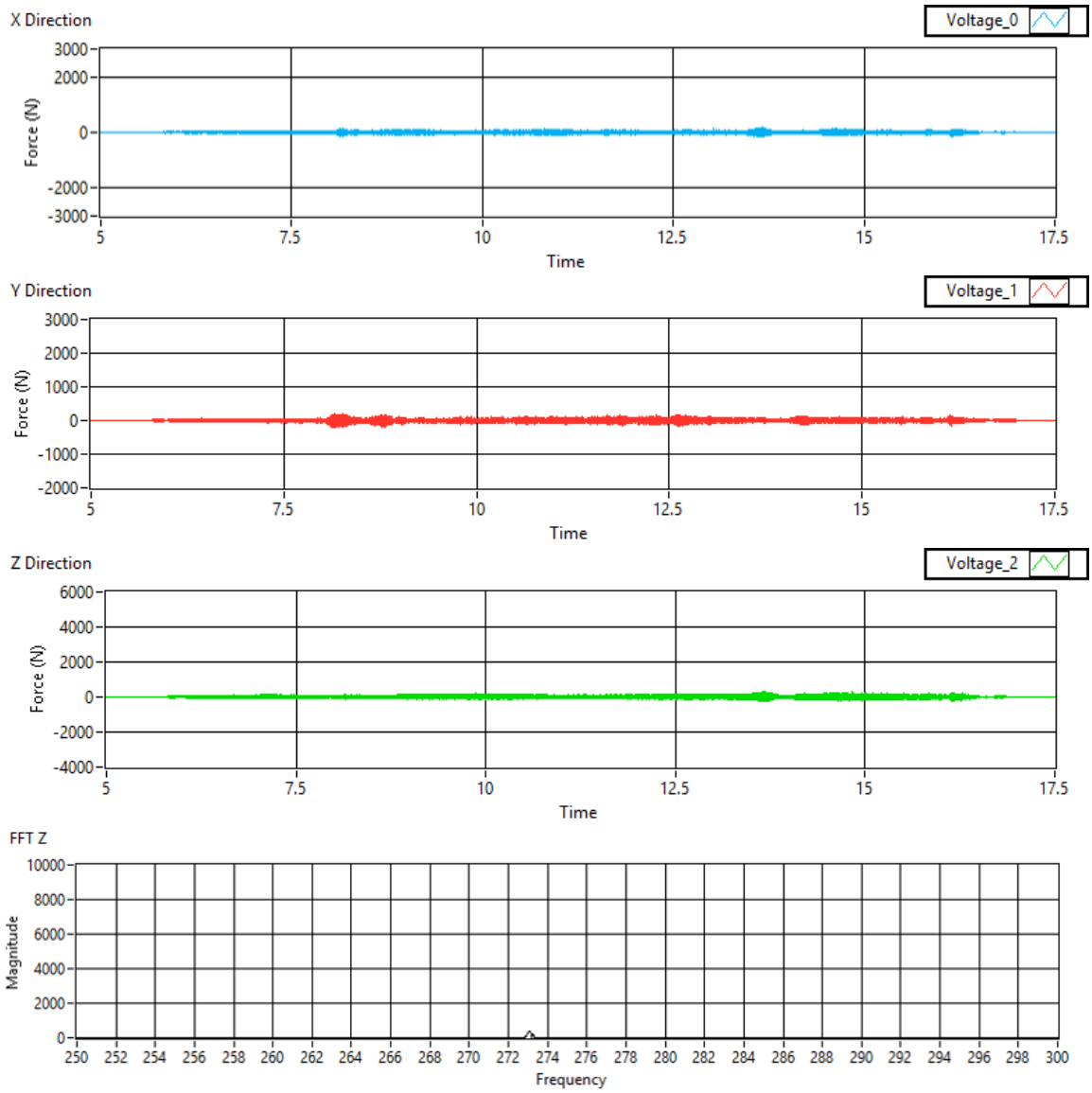

Figure 4.13: Measured machining forces in the X Y and Z directions during damped machining of the flat plate, along with the Fast Fourier Transform of the Z direction force

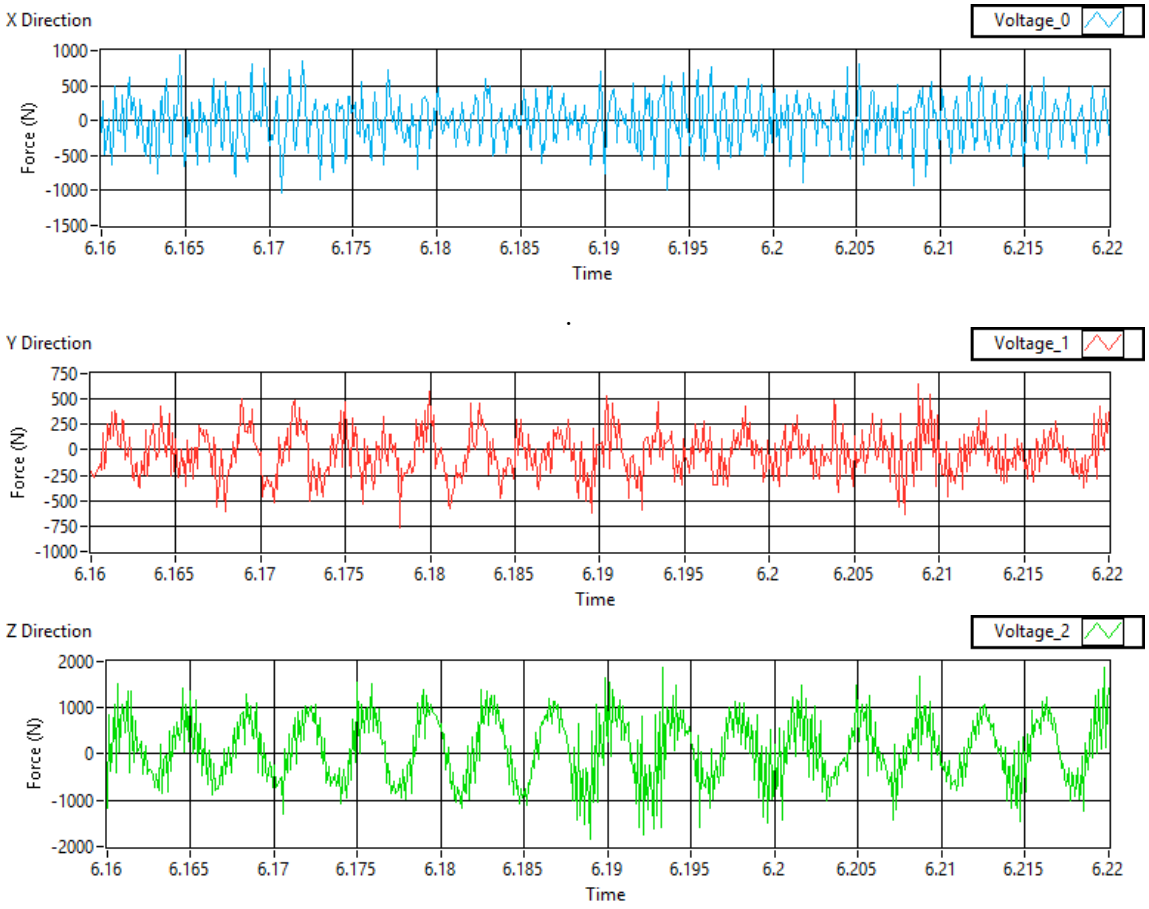

Figure 4.14: Smaller time increments of the measured X, Y, and Z forces for the undamped case

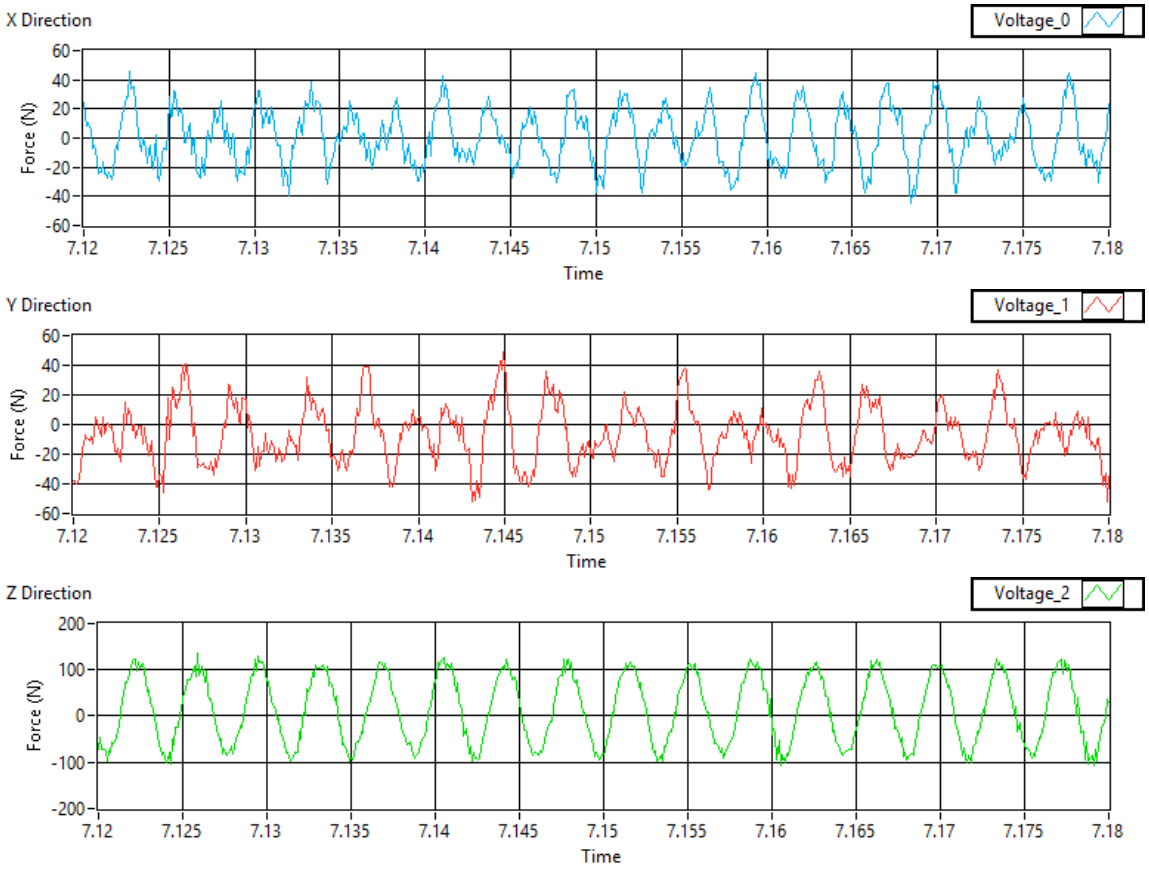

Figure 4.15: Smaller time increments of the measured X, Y, and Z forces for the damped case

Table 4.7: Interferometer roughness measurements on damped and undamped flat plate workpieces

Location	Undamped Part R_a (μm)	Damped Part R_a (μm)
A1	13.579	1.831
A2	7.482	0.637
A3	17.016	0.579
A4	57.908	0.494
A5	33.473	0.826
B1	7.182	2.742
B2	22.192	0.504
B3	15.229	0.692
B4	53.150	1.080
B5	33.662	0.717
C1	14.253	1.235
C2	10.325	0.619
C3	17.358	0.532
C4	23.010	0.886
C5	39.528	1.668
D1	27.250	0.694
D2	52.600	0.462
D3	13.230	0.776
D4	23.126	2.240
D5	19.288	1.100
Average	25.042	1.016
Standard Deviation	15.372	0.633

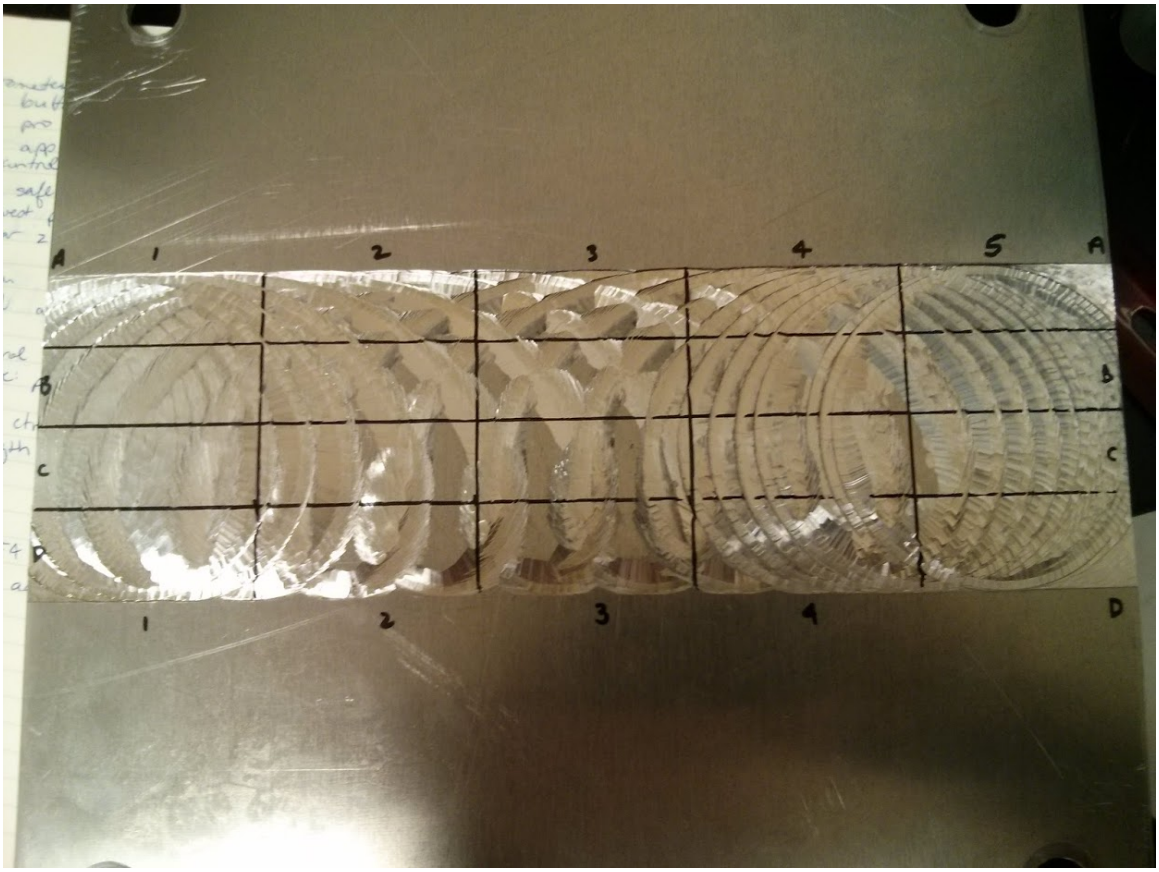

Figure 4.16: Flat plate surface roughness measurement locations; columns are designated 1 through 5 from left to right and rows are designated A through D from top to bottom

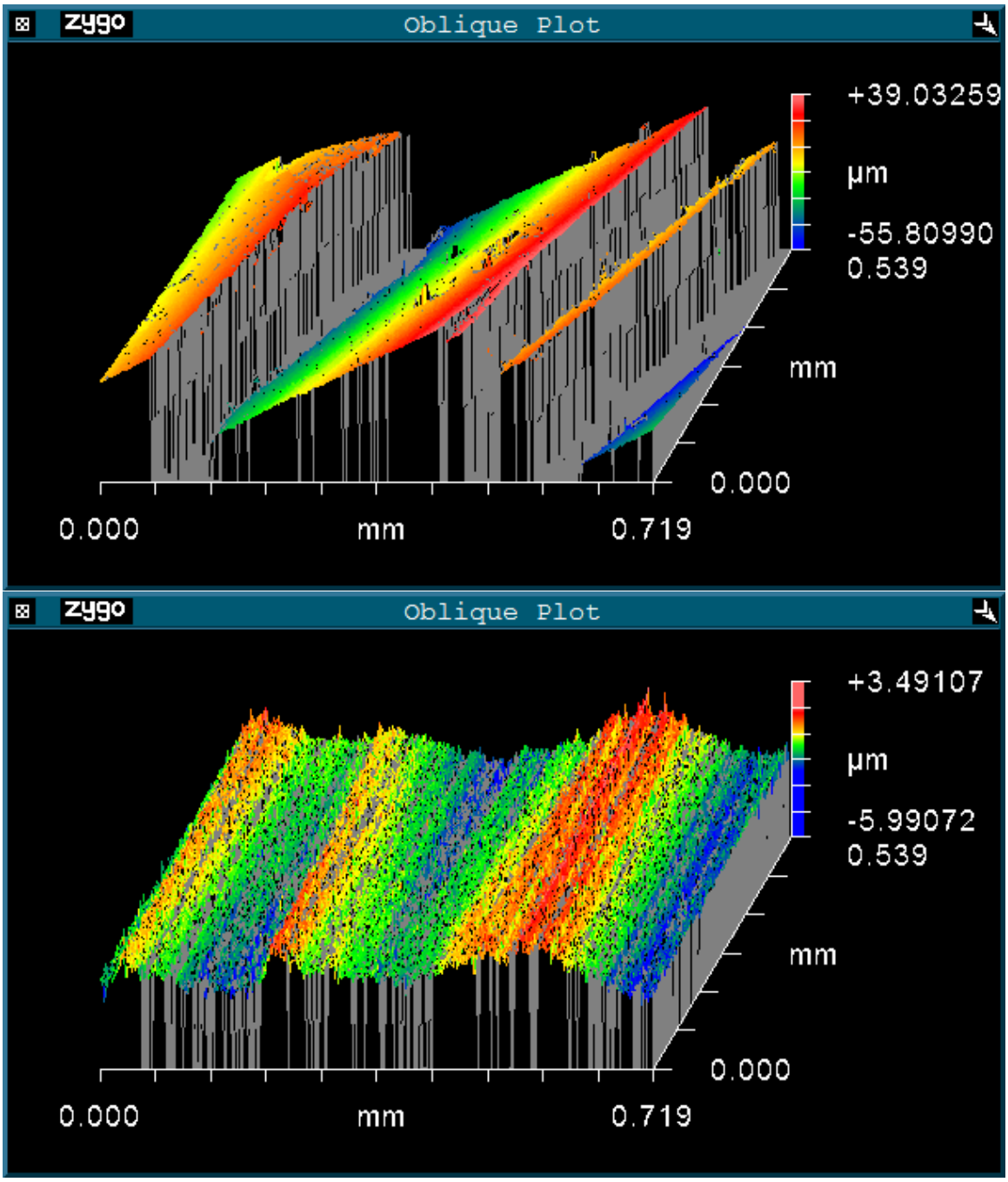

Figure 4.17: Surface profile captured by interferometer for location C3 on the undamped plate (top) and location B3 on the damped plate (bottom)

As with the c-channel test, the R_a values for the undamped case are much higher than for the magnetically damped case, in this test by 23.6 times. The standard deviation is also much higher for the undamped case, once again indicating that the addition of damping results in a more consistent machined surface.

In this test, it is interesting to note that the damped part had a better surface finish in the middle of the machining pass, while the undamped part had a better surface finish towards the edges. Eliminating the surface finish measurements from columns 1 and 5, the average surface R_a value for the undamped case becomes 26.052 with a standard deviation of 17.882: a slightly rougher, less consistent surface. For the damped case, the R_a value becomes 0.791 with a standard deviation of 0.491: a smoother, more consistent surface.

Chapter 5

Conclusion

Thin-walled and thin-floored parts, commonly machined in industry, have the potential to experience excessive vibration during machining. This vibration can be attenuated through the addition of damping. A useful non-contact method is the use of eddy current damping. A thin tab can either be affixed to the underside of the workpiece, or left during previous machining operations if applicable. Magnets can be arranged underneath the minimally-supported part in such a way as to allow the thin tab to move between the magnets as machining-induced vibrations occur. This movement generates eddy currents which dissipate energy and lessen the amplitude of vibration.

The results of the c-channel machining test, a favourable configuration for the addition of eddy current damping, indicated that the damping was sufficient to noticeably reduce vibrations in a machining scenario. A test was then conducted on a more realistic thin plate workpiece supported at the four corners. An aluminum tab was welded to the workpiece and allowed to vibrate freely between two magnets, situated underneath the workpiece.

The workpiece without the addition of eddy current damping experienced cutting forces 10 times as high as that with eddy current damping, and the average R_a value measured at various locations across the machined surface was 25 times as high with a higher standard deviation. The use of eddy current damping therefore resulted in a significant decrease in the cutting forces, which is indicative of favourable cutting conditions. It also produced a significantly smoother and more consistent surface finish, which is desirable in machining.

5.1 Future Work

While the surface attained with the use of eddy current damping was drastically improved from the undamped case, further improvements are still possible. In particular, increased vibration was observed at the beginning and end of the cut, away from the location of the eddy current damping. On the finished part, the surface finish was noticeably better in the centre of the damped part, and towards the edges of the undamped part. This suggests that the effect of the magnetic damping is considerable but localized, and that the addition of more magnets along the length of cut would be beneficial.

The magnet configuration in which the conductive material moves towards and away from the surface of the magnet rather than in the same plane would be convenient for machining. Unfortunately, cantilever beam tests did not indicate that the damping effect was strong enough for the magnets used. Since this configuration is considerably weaker, much stronger magnets would need to be used in order to achieve the same benefit. This introduces logistical problems related to magnet handling. These may be somewhat lessened with the use of an electro-magnet, which

could easily be turned off during setup and removal of the fixture.

Bibliography

Ahmadi, K. and Ismail, F. (2010a). Experimental investigation of process damping nonlinearity in machining chatter. *International Journal of Machine Tools and Manufacture*, **50**(11), 1006 – 1014.

Ahmadi, K. and Ismail, F. (2010b). Machining chatter in flank milling. *International Journal of Machine Tools and Manufacture*, **50**(1), 75 – 85.

Ahmadi, K. and Ismail, F. (2011). Analytical stability lobes including nonlinear process damping effect on machining chatter. *International Journal of Machine Tools and Manufacture*, **51**(4), 296 – 308.

Altintas, Y. and Budak, E. (1995). Analytical prediction of stability lobes in milling. *CIRP Annals - Manufacturing Technology*, **44**(1), 357 – 362.

Altintas, Y., Eynian, M., and Onozuka, H. (2008). Identification of dynamic cutting force coefficients and chatter stability with process damping. *CIRP Annals - Manufacturing Technology*, **57**(1), 371 – 374.

Bae, J.-S., Kwak, M. K., and Inman, D. J. (2005). Vibration suppression of a cantilever beam using eddy current damper. *Journal of Sound and Vibration*, **284**(35), 805 – 824.

Benardos, P. and Vosniakos, G.-C. (2003). Predicting surface roughness in machining: a review. *International Journal of Machine Tools and Manufacture*, **43**(8), 833 – 844.

Budak, E. and Tunc, L. (2010). Identification and modeling of process damping in turning and milling using a new approach. *CIRP Annals - Manufacturing Technology*, **59**(1), 403 – 408.

Campa, F., Seguy, S., de Lacalle, L. L., Arnaud, L., Dessein, G., and Aramendi, G. (2007). Stable milling of thin-walled parts with variable dynamics. In *6th International Conference on High Speed Machining*.

Chen, W., Ni, L., and Xue, J. (2008). Deformation control through fixture layout design and clamping force optimization. *The International Journal of Advanced Manufacturing Technology*, **38**(9-10), 860–867.

Daimon, M., Yoshida, T., Kojima, N., Yamamoto, H., and Hoshi, T. (1985). Study for designing fixtures considering dynamics of thin-walled plate- and box-like workpieces. *CIRP Annals - Manufacturing Technology*, **34**(1), 319 – 322.

Das, A., Nandi, A., and Neogy, S. (2008). Application of finite elements for determination of the damping coefficient of an eddy current damper using Matlab. *International Journal of Mechanical Engineering Education*, **36**(2), 120 – 139.

Davis, L. C. and Reitz, J. R. (1971). Eddy currents in finite conducting sheets. *Journal of Applied Physics*, **42**(11), 4119–4127.

De Meter, E. C. and Hockenberger, M. J. (1997). The application of tool path compensation for the reduction of clampinginduced geometric errors. *International Journal of Production Research*, **35**(12), 3415–3432.

De Meter, E. C., Xie, W., Choudhuri, S., Vallapuzha, S., and Trethewey, M. W. (2001). A model to predict minimum required clamp pre-loads in light of fixture-workpiece compliance. *International Journal of Machine Tools and Manufacture*, **41**(7), 1031 – 1054.

Duncan, G., Tummond, M., and Schmitz, T. (2005). An investigation of the dynamic absorber effect in high-speed machining. *International Journal of Machine Tools and Manufacture*, **45**(45), 497 – 507.

Ebrahimi, B., Khamesee, M., and Golnaraghi, F. (2010). Permanent magnet configuration in design of an eddy current damper. *Microsystem Technologies*, **16**(1-2), 19–24.

Eksioglu, C., Kilic, Z. M., and Altintas, Y. (2012). Discrete-time prediction of chatter stability, cutting forces, and surface location errors in flexible milling systems. *Journal of Manufacturing Science and Engineering*, **134**(6), 13.

Ganguli, A., Deraemaeker, A., Horodinca, M., and Preumont, A. (2005). Active damping of chatter in machine tools - demonstration with a hardware-in-the-loop simulator. *Proceedings of the Institution of Mechanical Engineers, Part I: Journal of Systems and Control Engineering*, **219**(5), 359–369.

Ganguli, A., Deraemaeker, A., and Preumont, A. (2007). Regenerative chatter reduction by active damping control. *Journal of Sound and Vibration*, **300**(35), 847 – 862.

Hamade, R., Seif, C., and Ismail, F. (2006). Extracting cutting force coefficients from drilling experiments. *International Journal of Machine Tools and Manufacture*, **46**(34), 387 – 396.

Huang, C. and Wang, J.-J. J. (2011). Effects of cutting conditions on dynamic cutting factor and process damping in milling. *International Journal of Machine Tools and Manufacture*, **51**(4), 320 – 330.

Kanamori, M. and Ishihara, Y. (1989). Finite element analysis of an electromagnetic damper taking into account the reaction of the magnetic field. *JSME international journal. Ser. 3, Vibration, control engineering, engineering for industry*, **32**(1), 36–43.

Kaya, N. (2006). Machining fixture locating and clamping position optimization using genetic algorithms. *Computers in Industry*, **57**(2), 112 – 120.

Lee, B., Tarng, Y., and Ma, S. (1995). Modeling of the process damping force in chatter vibration. *International Journal of Machine Tools and Manufacture*, **35**(7), 951 – 962.

Li, B. and Melkote, S. (2001a). Fixture clamping force optimisation and its impact on workpiece location accuracy. *The International Journal of Advanced Manufacturing Technology*, **17**(2), 104–113.

Li, B. and Melkote, S. N. (1999). Improved workpiece location accuracy through fixture layout optimization. *International Journal of Machine Tools and Manufacture*, **39**(6), 871 – 883.

Li, B. and Melkote, S. N. (2001b). Optimal fixture design accounting for the effect of workpiece dynamics. *The International Journal of Advanced Manufacturing Technology*, **18**(10), 701–707.

Li, B., Melkote, S. N., and Liang, S. Y. (2000). Analysis of reactions and minimum clamping force for machining fixtures with large contact areas. *The International Journal of Advanced Manufacturing Technology*, **16**(2), 79–84.

Liu, X. and Cheng, K. (2005). Modelling the machining dynamics of peripheral milling. *International Journal of Machine Tools and Manufacture*, **45**(11), 1301 – 1320.

Lu, C. (2008). Study on prediction of surface quality in machining process. *Journal of Materials Processing Technology*, **205**(13), 439 – 450.

Manufacturing Automation Laboratories Inc (2011). Cutpro 8.0. http://www.malinc.com/index.html.

Nagaya, K., Kojima, H., Karube, Y., and Kibayashi, H. (1984). Braking forces and damping coefficients of eddy current brakes consisting of cylindrical magnets and plate conductors of arbitrary shape. *Magnetics, IEEE Transactions on*, **20**(6), 2136–2145.

Niho, T. and Horie, T. (2010). Non-contact control of elastic vibration with magnetic damping for non-ferromagnetic plate. *International Journal of Applied Electromagnetics and Mechanics*, **34**(4), 249 – 264.

Quintana, G. and Ciurana, J. (2011). Chatter in machining processes: A review. *International Journal of Machine Tools and Manufacture*, **51**(5), 363 – 376.

Rahnama, R., Sajjadi, M., and Park, S. S. (2009). Chatter suppression in micro end milling with process damping. *Journal of Materials Processing Technology*, **209**(17), 5766 – 5776.

Ratchev, S., Liu, S., Huang, W., and Becker, A. (2004). Milling error prediction and compensation in machining of low-rigidity parts. *International Journal of Machine Tools and Manufacture*, **44**(15), 1629 – 1641.

Rivin, E. I. and Kang, H. (1989). Improvement of machining conditions for slender parts by tuned dynamic stiffness of tool. *International Journal of Machine Tools and Manufacture*, **29**(3), 361 – 376.

Sakurai, H. (1992). Automatic setup planning and fixture design for machining. *Journal of Manufacturing Systems*, **11**(1), 30 – 37.

Sellmeier, V. and Denkena, B. (2012). High speed process damping in milling. *CIRP Journal of Manufacturing Science and Technology*, **5**(1), 8 – 19.

Singh, R., Sharma, M., and Singh, V. (2012). An experimental study of vibration control of cantilever beam using eddy current damper. *International Journal of Applied Engineering Research*, **7**(11), 1491 – 1496.

Sodano, H. A. (2005). *Development of novel eddy current dampers for the suppression of structural vibrations*. Ph.D. thesis, Virginia Polytechnic Institute and State University.

Sodano, H. A. and Bae, J.-S. (2004). Eddy current damping in structures. *The Shock and Vibration Digest*, **36**(6), 469 – 478.

Sodano, H. A., Bae, J.-S., Inman, D. J., and Belvin, W. K. (2005). Concept and model of eddy current damper for vibration suppression of a beam. *Journal of Sound and Vibration*, **288**(45), 1177 – 1196.

Sodano, H. A., Inman, D. J., and Belvin, W. K. (2006a). Development of a new passive-active magnetic damper for vibration suppression. *Transactions of the ASME*, **128**, 318 – 327.

Sodano, H. A., Bae, J.-S., Inman, D. J., and Belvin, W. K. (2006b). Improved concept and model of eddy current damper. *Journal of Vibration and Acoustics*, **128**(3), 294 – 302.

Sodano, H. A., Bae, J.-S., Inman, D. J., and Belvin, W. K. (2006c). Modeling and application of eddy current damper for suppression of membrane vibrations. *American Institute of Aeronautics and Astronautics Journal*, **44**(3), 541 – 549.

Song, Q. H., Wan, Y., Yu, S. Q., Ai, X., and Pang, J. (2009). Stability prediction during thin-walled workpiece high-speed milling. *Advanced Materials Research*, **69**, 428–432.

Suh, J. D., Chang, S. H., Lee, D. G., Choi, J. K., and Park, B. S. (2001). Damping characteristics of composite hybrid spindle covers for high speed machine tools. *Journal of Materials Processing Technology*, **113**(13), 178 – 183. 5th Asia Pacific conference on Materials processing.

Tanaka, Y. and Horie, T. (2002). Characteristics of the forced vibration with magnetic damping. *International Journal of Applied Electromagnetics and Mechanics*, **13**(1), 45 – 51.

Tang, A. and Liu, Z. (2009). Three-dimensional stability lobe and maximum material removal rate in end milling of thin-walled plate. *The International Journal of Advanced Manufacturing Technology*, **43**(1-2), 33–39.

Tlusty, J. and Ismail, F. (1981). Basic non-linearity in machining chatter. *CIRP Annals - Manufacturing Technology*, **30**(1), 299 – 304.

Tunç, L. and Budak, E. (2012). Effect of cutting conditions and tool geometry on process damping in machining. *International Journal of Machine Tools and Manufacture*, **57**(0), 10 – 19.

Wang, M. (2011). Feasibility study of nonlinear tuned mass damper for machining chatter suppression. *Journal of Sound and Vibration*, **330**(9), 1917 – 1930.

Weck, M., Hennes, N., and Krell, M. (1999). Spindle and toolsystems with high damping. *CIRP Annals - Manufacturing Technology*, **48**(1), 297 – 302.

Yang, Y., Xu, D., and Liu, Q. (2015a). Milling vibration attenuation by eddy current damping. *International Journal of Advanced Manufacturing Technology*.

Yang, Y., Xu, D., and Liu, Q. (2015b). Vibration suppression of thin-walled workpiece machining based on electromagnetic induction. *Materials and Manufacturing Processes*, **0**(0), 1–7.

Yusoff, A., Turner, S., Taylor, C., and Sims, N. (2010). The role of tool geometry in process damped milling. *The International Journal of Advanced Manufacturing Technology*, **50**(9-12), 883–895.

Zhang, Y. and Sims, N. D. (2005). Milling workpiece chatter avoidance using piezoelectric active damping: a feasibility study. *Smart Materials and Structures*, **14**(6), N65.

Zuo, L. (2005). *Element and system design for active and passive vibration isolation*. Ph.D. thesis, Massachusetts Institute of Technology.